ANL-77-92

PHYSICS OF REACTOR SAFETY

Quarterly Report

July–September 1977

ARGONNE NATIONAL LABORATORY, ARGONNE, ILLINOIS

Prepared for the U. S. NUCLEAR REGULATORY COMMISSION
under Contract W-31-109-Eng-38

The facilities of Argonne National Laboratory are owned by the United States Government. Under the terms of a contract (W-31-109-Eng-38) between the U. S. Department of Energy, Argonne Universities Association and The University of Chicago, the University employs the staff and operates the Laboratory in accordance with policies and programs formulated, approved and reviewed by the Association.

MEMBERS OF ARGONNE UNIVERSITIES ASSOCIATION

The University of Arizona
Carnegie-Mellon University
Case Western Reserve University
The University of Chicago
University of Cincinnati
Illinois Institute of Technology
University of Illinois
Indiana University
Iowa State University
The University of Iowa
Kansas State University
The University of Kansas
Loyola University
Marquette University
Michigan State University
The University of Michigan
University of Minnesota
University of Missouri
Northwestern University
University of Notre Dame
The Ohio State University
Ohio University
The Pennsylvania State University
Purdue University
Saint Louis University
Southern Illinois University
The University of Texas at Austin
Washington University
Wayne State University
The University of Wisconsin

Printed in the United States of America
Available from
National Technical Information Service
U. S. Department of Commerce
5285 Port Royal Road
Springfield, Virginia 22161
Price: Printed Copy $4.50; Microfiche $3.00

Distribution Category:
Advanced Reactor Safety
Research—Fast Reactors
(NRC-7)

ANL-77-92

ARGONNE NATIONAL LABORATORY
9700 South Cass Avenue
Argonne, Illinois 60439

PHYSICS OF REACTOR SAFETY

Quarterly Report
July—September 1977

Applied Physics Division

December 1977

Work performed for the
Division of Reactor Safety Research
U. S. Nuclear Regulatory Commission

Previous reports in this series

ANL-77-9	July—September 1976
ANL-77-22	October—December 1976
ANL-77-48	January—March 1977
ANL-77-69	April—June 1977

TABLE OF CONTENTS

LIST OF FIGURES

LIST OF FIGURES (Cont)

LIST OF TABLES

PHYSICS OF REACTOR SAFETY

Quarterly Report
July—September 1977

ABSTRACT

This quarterly progress report summarizes work done in Argonne National Laboratory's Applied Physics Division and Components Technology Division for the Division of Reactor Safety Research of the U. S. Nuclear Regulatory Commission during the months of July-September 1977. The work in the Applied Physics Division includes reports on reactor safety program by members of the Reactor Safety Appraisals Group, Monte Carlo analysis of safety-related critical assembly experiments by members of the Theoretical Fast Reactor Physics Group, and planning of safety-related (ZPR) Planning and Experiments Group. Work on reactor core thermal-hydraulic code development performed in the Components Technology Division is also included in this report.

I. TECHNICAL COORDINATION - FAST REACTOR SAFETY ANALYSIS (A2015)

A. Summary

It has been found that the major benefits of the distributed-particle-in-cell technique in FX2-POOL can be obtained by using two particles per dimension per cell.

Linking of EPIC to SAS3D is complete to the point that a single channel module is now running.

Studies with TWO-POOL of the importance of modeling assumptions for calculations of disassembly in a HCDA have shown that vapor-liquid slip is not important but that accident energetics are quite sensitive to liquid droplet size if fuel vaporization and condensation are limited by thermal conduction.

A review of out-of-pile burst failure tests on irradiated fuel pin cladding has indicated that the most satisfactory way to characterize the results is in terms of the decrease in failure temperature from that of unirradiated cladding at the same failure stress. This decrease ranges from -100 to 400°F, with no correlation with fluence, irradiation temperature, or failure temperature.

B. Study of Basic Problems in Accident Analysis

1. FX2-POOL Development (P. B. Abramson)

A generalized version of FX2-POOL using variable mesh and variable number of particles in the DPIC (distributed particle-in-Cell)[1] routines was written. It was found that the major benefits of using DPIC techniques can be obtained by using two particles per dimension per cell. This allows the major "fine structure" effects to be seen in the macroscopic variables such as work energy (Figure 1) and contributes a negligible cost to computational time (whereas using four particles per dimension per cell causes approximately a 30% increase in computing costs).

The generalized code should be available for release by the first of the year and will include all options in the POOLVENS calculation including selecting either the new pressure formulation for incompressible cells[2] on the "chewing gum" model[3] (in which axial and radial incompressible motions are decoupled and the choice of stochastic with input distribution functions vs. fixed values for the heat transfer parameters as well as the isentopic work energy routines.

2. Behrens Effect (P. B. Abramson)

A co-operative study of the bubble collapse effect on accident energetics was initiated with E. L. Fuller (EPRI).

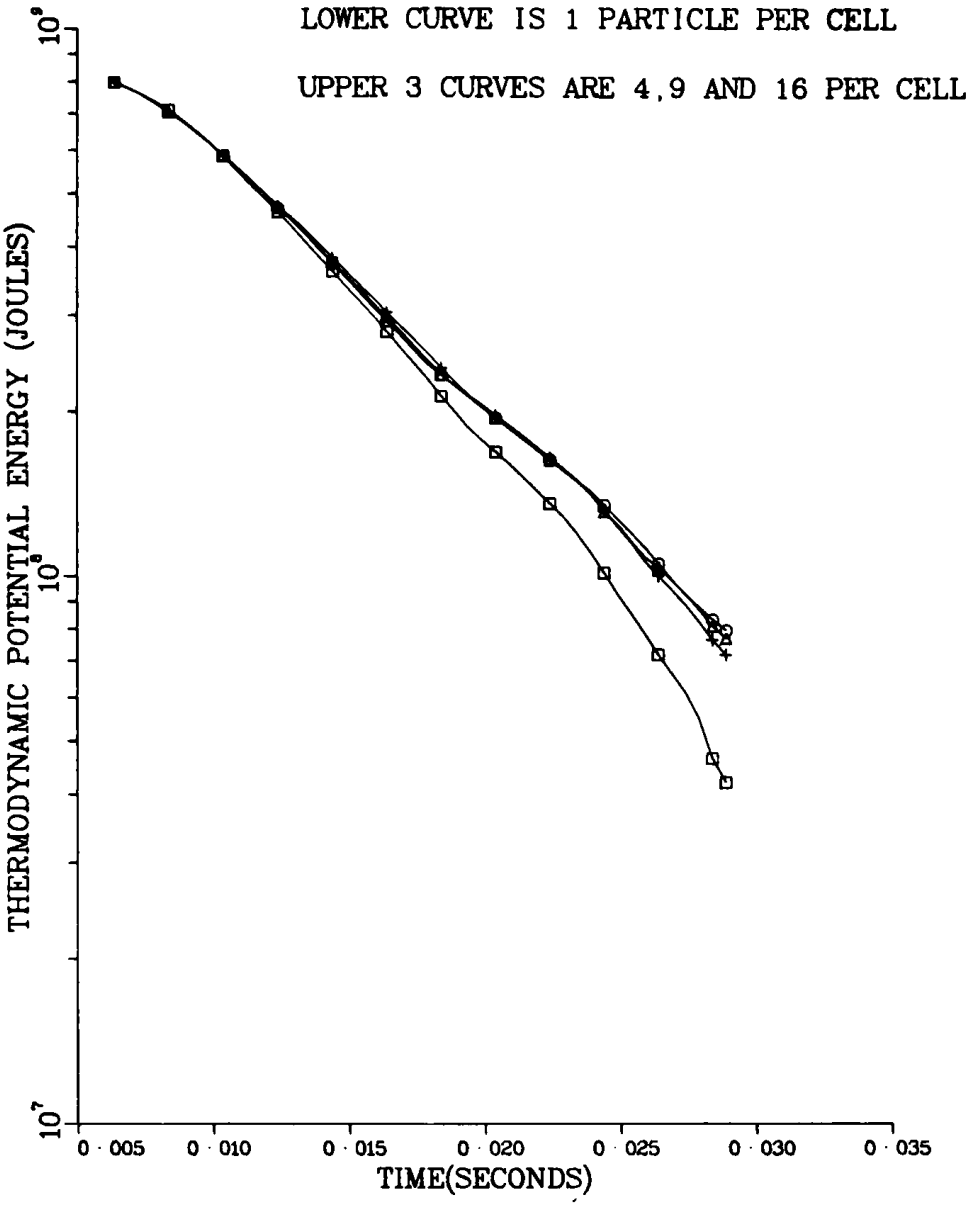

Fig. 1. Effect of Number of DPIC Particles
ANL Neg. No. 116-77-940.

3. EPIC (P. A. Pizzica and P. B. Abramson)

a) Hook up of EPIC to SAS3D is continuing with a simple channel module now running.

b) Advice was given to M. A. Young (SANDIA) on proper application of EPIC to ACPR experiments.

4. FX2-TWOPOOL (J. J. Sienicki)

Studies were performed with FX2-TWOPOOL to scope the importance of several modeling assumptions during the prompt burst portion of disassembly. The reactor model chosen for this investigation was based upon CRBR geometry and was assumed to be completely voided of sodium. The results indicated that for the prompt burst portion of an HCDA:

a) Vapor-liquid slip plays a relatively insignificant role in establishing energetics, implying that analyses that do not model vapor-liquid slip may be adequate. Furthermore, if conditions of saturation are assumed to be maintained, calculations that do not permit vapor-liquid slip appear to be conservative.

b) The modeling of conduction limited fuel vaporization and condensation causes the energetics to be highly sensitive to variations in the droplet size (i.e. in the parametric values) for the sizes of interest in HCDA analysis. Care must therefore be exercised in the inclusion of this phenomenon in energetics calculations.

c) Insignificant differences are observed between the use of space-time kinetics (quasistatic diffusion theory) and point kinetics, indicating again that point kinetics is normally adequate for analysis of the prompt burst portion of an HCDA.

d) No significant differences were found to results from assuming that delayed neutron precursors remain stationary where they are created rather than assuming that they move together with fuel.

5. Review of Burst Rupture Stress of Unirradiated and Irradiated 20% Cold Worked 316 Stainless Steel Cladding During Transient Heating (Kalimullah and H. H. Hummel)

(a) Introduction. In order to calculate reliably failure conditions in an overpower transient for irradiated fuel pin cladding it is necessary to be able to characterize the strength of the cladding as a function of failure temperature, heating rate, irradiation temperature, and fast fluence. It is important to be able to state error limits for such characterization in order that discrepancies between calculated and experimental failure conditions resulting from model deficiencies rather than from uncertainties in clad properties can be identified. Existing analyses of out-of-pile experiments of failure of irradiated clad by internal gas pressurization are unsatisfactory in that they do not identify the uncertainties very clearly, and also tend to use the life fraction rule for predicting failure. The latter seems inappropriate at this time as will be explained presently, and a burst rupture stress criterion seems preferable. The present study was undertaken to establish failure uncertainty limits with such a characterization of clad strength.

(b) Review of Earlier Analysis. It was found in Reference 4 that the ratio of the rupture stress of the irradiated cladding to that of unirradiated cladding at the same (failure) temperature does not correlate well with the irradiation temperature. In this evaluation, the effect of variation of fast fluence in the range $1.6\text{-}4.0 \times 10^{22}$ neutrons/cm^2 was assumed to be small. In Reference 5 it was found that the decrease in failure temperature at the same stress due to irradiation, and hence the rupture stress at the same failure temperature, does not correlate well with the fast fluence. In this evaluation, the effect of variation of the irradiation temperatures in the range 700-1000°F was assumed to be small. While the findings of the references 4 and 5 are certainly correct, it is found in the present review that a plot of the decrease in failure temperature vs. irradiation temperature for almost equal fast fluences (in the range $1.90\text{-}2.25 \times 10^{22}$ neutrons/cm^2) also shows wide scatter. In this state of the art, it is appropriate to use the

conceptually most simple failure criterion for which the uncertainty could be easily bounded. (For example, if one chose a plastic strain failure criterion, one should be able to compute the plastic strain of the irradiated cladding and also should ascertain the range of the plastic strain in which failure will certainly occur.) Undoubtedly, the most simple of the failure criteria is the rupture stress criterion, and in this review an empirical fit to the rupture stress of the irradiated cladding is suggested using the decrease in failure temperature as an uncertain parameter. A range of this parameter is suggested in which failure will certainly occur. A failure criterion based on the rule that the amount of life expended in any time interval is independent of the life expended in the rest of the time-temerpature-stress profile, i.e. the life fraction rule, using, for example, the Larson-Miller parameter or Sherby-Orr-Dorn parameter, etc., is not appropriate at present because of the following reasons: (a) The life fraction rule is not yet experimentally verified for rupture lives of the order of fractions of a second and obviously it is difficult to do. Reasonable confidence in the rule is reported in the literature only for rupture lives of the order of one hour to several thousand hours. Unless the rule is reasonably verified for small rupture lives also, the generalization that the rule provides for predicting failure in various time-temperature-stress profiles different from the base experiments will not be very reliable. (b) All the coefficients in a failure correlation based on this rule will depend upon irradiation temperature, fast fluence and other variables which may determine the nature of the material obtained after irradiation. The insufficiency and the scatter of the available test data makes it difficult to determine the dependence of these coefficients on irradiation variables and to put the needed upper and lower bounds on these coefficients to completely cover the scatter. A correlation with such bands determined for more than a couple of the coefficients will be hard to use. (c) In References 6 and 7 failure criteria based on life fraction rule and Larson-Miller parameter for unirradiated cladding and some irradiated claddings have been reported. These failure correlations were developed from FCTT data assuming that all the rupture life accumulates in a small fraction of the transient test when the specimen temperature approaches the failure temperature, and this assumption implies that the failure stress is a function of the failure temperature and the heating rate (see Eqs. (16) and (17) of Reference 6), i.e. the most simple stress failure criterion. At the present state of affairs, these Larson-Miller parameter failure correlations are no better than the simple stress failure criterion and do not represent the intended generalizations for use in time-temperature-stress profiles different from the base experiments.

(c) Reanalysis of Data in Terms of Burst Rupture Stress. Table I shows the experimental burst rupture stress of unirradiated 20% cold worked 316 stainless steel cladding during transient heating rates of 10°F/sec and 200°F/sec. The experimental values have been obtained from smooth curves (one for each heating rate) drawn through all the FCTT data[4] points on a failure temperature-failure hoop stress graph paper. These experimental values for the two heating rates are not very different at low temperatures but the difference is significant at higher temperatures (the temperature range over which cladding failure most likely may occur in a transient overpower accident). Since heating rates of 200°F/sec or even considerably larger are typical of LMFBR transient overpower accidents, and extrapolations of failure stress for higher heating rates from the values of failure stress at these two heating rates may be misleading, it seems appropriate at present to use the 200°F/sec data for all LMFBR TOP analyses no matter what heating rates are

TABLE I. Unirradiated 20% Cold Worked 316 Stainless Steel Cladding Burst Rupture Stress During Transient Heating

Serial No.	Failure Temp. °F	Failure Hoop Stress at 200°F/sec, Ksi		Failure hoop Stress at 10°F/sec, Ksi	Yield Stress[7] Ksi
		Experimental[4]	Eq. (1)	Experimental[4]	
1	800	102.5		105.0	75.71
2	1000	98.3	97.5	97.5	71.75
3	1200	88.0	89.9	86.0	55.57
4	1400	70.0	71.3	65.0	31.97
5	1600	49.0	49.0	41.7	17.42
6	1700	38.2	38.5	31.8	
7	1800	29.1	29.2	22.5	13.94*
8	1900	20.4	21.4	15.0	
9	2000	14.4	15.1	9.6	10.45*
10	2100	10.5	10.3	6.0	
11	2200	7.2	6.8	4.0	6.97*
12	2300	4.8	4.4	2.4	
13	2400	3.0	2.7	1.3	3.48*
14	2500	1.4	1.6	0.6	1.74*

*Linearly interpolated between the yield stresses of 17.42 Ksi at 1600°F and zero at the melting point of 2600°F.

encountered. The following equation adequately correlates the 200°F/sec data for the unirradiated cladding above 1000°F:

$$\sigma_f = 97.5 \exp\left(-1.864x^{1.95}\right), \quad (1)$$

where σ_f = failure stress at 200°F/sec, Ksi,

x = T/1000 - 1, and

T = failure temperature, °F.

This correlation is compared with the experimental values in Table I. The FCTT data for diametral plastic strain at failure for the unirradiated cladding above 1000°F during the 200°F/sec heating rate is approximated by the following correlation:

$$\varepsilon_f(\%) = (0.5 + 4.62x^{2.4}) \exp\left(-0.185x^7\right). \quad (2)$$

Due to the scatter of availabe data,[4] especially above 2000°F, the maximum difference between Eq. (2) and the test values is about ±30%. The plastic

strains at failure given by Eq. (2) range from a few tenths of a percent to more than 4%. During the 10°F/sec heating rate the failure strains are higher and range from a few tenths of a percent to more than 8%.[4] Table I also shows the 0.2% yield stress of unirradiated 20% cold worked 316 stainless steel[8] which is considerably lower than the failure stress for the 200°F/sec heating rate.

The failure stress and strain of irradiated 20% cold worked 316 stainless steel cladding during transient heating have large uncertainties with respect to their variation with fast neutron fluence (E > 0.1 MeV) and the irradiation temperature. Besides irradiation damage, sodium-attack and fuel-attack also reduce the failure stress and strain of the irradiated cladding.[4,5] Table II summarizes some FCTT burst test results[5] for 20% cold worked 316 stainless steel irradiated to fluences in the range 1.90-3.65 × 10^{22} neutrons/cm^2 at

TABLE II. FCTT Burst Test Results for Irradiated Cladding Specimens from NUMEC and PNL Pins Over the Fueled Region at a Heating Rate of 200°F/sec.[5]

Case	Average Fluence 10^{22}n/cm^2	Midwall Irradiation Temp. °F	Irradiated Failure Temp. °F	Failure Stress Ksi	Unirradiated Failure Temp. °F	Decrease in Failure Temp. due to Irradiation, °F
1	3.05	890	1940	18.0	1940	0
2	2.90	800	1670	28.8	1803	133
3	3.05	935	1525	28.8	1803	278
4	2.15	743	1520	43.8	1648	128
5	1.90	933	1490	43.2	1654	164
6	2.40	781	1210	72.0	1378	168
7	3.05	870	1310	72.0	1378	68
8	1.95	983	1205	84.4	1240	35
9	1.90	995	1070	97.3	1019	-51
10	1.90	995	1140	76.1	1332	192
11	2.25	743	1120	97.2	1021	-99
12	2.80	930	1980	18.0	1940	-40
13	3.50	798	1770	28.8	1803	33
14	3.65	953	1400	28.8	1803	403
15	2.35	888	1230	72.0	1378	148

temperatures in the range 700-1000°F. All the cladding specimens comprising Table II were taken from the fueled portion of the pin (the test results for cladding specimens taken from the unfueled portion of the pin have been excluded) so that the appropriate effects of sodium-attack and fuel-attack are also accounted for. The test results[5] for the 10°F/sec heating rate were excluded from the table and only the data for 200°F/sec heating rate were included because the heating rates during LMFBR transient overpower accidents

are typically greater than 200°F/sec. These 15 test results have been plotted on a failure temperature-failure stress plane in Fig. 2. The fast neutron fluence, irradiation temperature and the decrease in the failure temperature relative to the unirradiated cladding at the same hoop stress are also shown below the points. From Fig. 2 it can be seen that the failure stress decreases as the failure temperature increases but any general trend for the combined effect of fluence, irradiation temperature, sodium-attack and fuel-attack on the failure stress at a given failure temperature is not clear. This combined effect of be quantified by the decrease in failure temperature relative to the unirradiated cladding at the same hoop stress. A plot of data points 4, 5, 8, 9, 10, and 11 of Table II, for specimens of almost equal fluences, on a decrease in failure temperature vs. midwall irradiation temperature graph paper

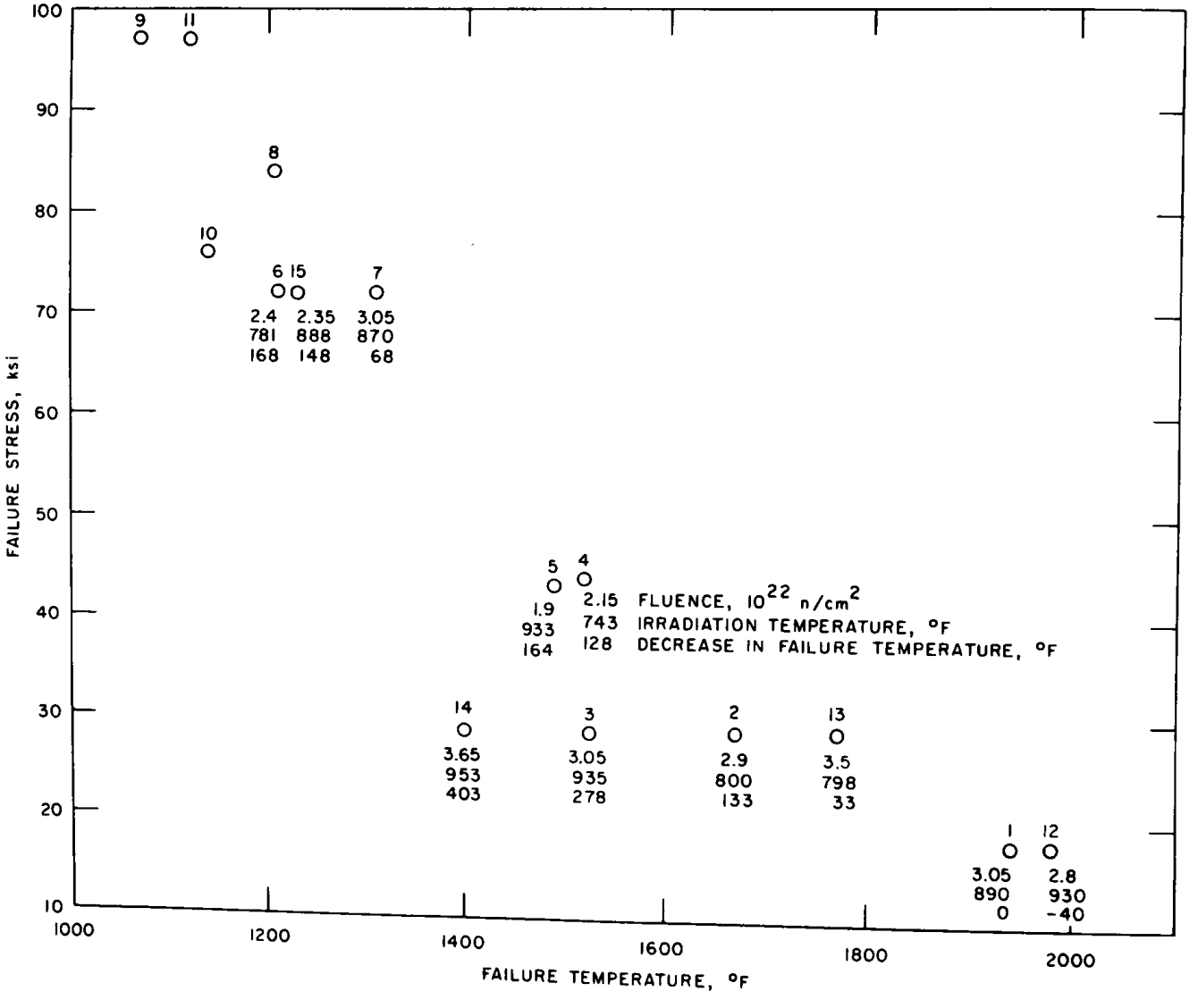

Fig. 2. FCTT Burst Test Results for Irradiated Cladding Specimens from NUMEC and PNL Pins Over Fueled Region at a Heating Rate of 200°F/sec. ANL Neg. No. 116-77-937

does not show any reasonable correlation. A plot of all the data points of Table II on a decrease in failure temperature vs. neutron fluence graph paper also shows wide scatter and no reasonable correlation. That these two plots show wide scatter implies that there are some unaccounted-for parameters, in addition to fluence and irradiation temperature, which have considerable effect on the cladding strength. (The temperature history of the specimen for the period of time after irradiation and before the FCTT test may influence its strength.) For the mechanistic failure analysis of irradiated fuel pins during transient overpower accidents, it seems appropriate at present to use the failure stress of the unirradiated cladding with a decrease in failure temperature due to irradiation. Table II shows that this decrease is uncertain within the range -100°F to 400°F, with no correlation with fluence, irradiation or failure temperature.

Examination of the strain at failure for the irradiated cladding shows that for fast neutron fluences greater than 1.0×10^{22} neutrons/cm^2 and failure stresses in the range 18-44 Ksi (corresponding to failure temperatures in the range 1400-1980°F) the diametral plastic strain is about 20% ± 6% (standard deviation) of the failure strain of the unirradiated cladding at the failure temperature of the irradiated cladding, and ranges from about 0.1 to 1.0%.

C. Coordination of RSR Fast Reactor Safety Research

P. Abramson visited LASL on July 14 to discuss SIMMER calculation with C. Bell, P. Alcouffe and R. Henninger and coordination/validation with M. Stevenson and J. Jackson.

P. Abramson visited SANDIA on July 15 to discuss SIMMER validation with R. Oslensen, R. Coats, J. Powell, W. Camp and J. Walker.

H. Hummel attended a SIMMER validation meeting on July 20 at LASL.

J. Sienicki and H. Hummel attended the ACRS W64 meeting on SIMMER at LASL on July 21-22.

H. Hummel and P. Abramson attended ACRS WG5 meeting in Washington on September 28 and 29.

H. Hummel and P. Pizzica attended a meeting of the WAC Comparative Studies Group in Brussels on September 21 and visited laboratories in Germany and England as part of our responsibilities with foreign implementing information exchange and cooperation fast reactor safety research program.

EPIC was transmitted to HEDL for their use.

PUBLICATIONS

An Explicit Iterative Technique for FX2
P. B. Abramson and T. A. Daly
June ANS meeting, New York, NY (June 12-16, 1977)

Comparison of the EPIC & PLUTO Computer Codes for TOP Conditions
P. A. Pizzica, J. J. Sienicki, P. B. Abramson and H. U. Wider
Trans. Am. Nuc. Soc., Vol 26 (June, 1977)

The Importance of Heat Transfer in Hypothetical Core Disruptive Accident Analysis
P. B. Abramson
Nuclear Technology, 35, Mid August 77, p. 87-96

A Numerical Model of Reactor Fuel and Coolant Motions Following Pin Failure
P. A. Pizzica and P. B. Abramson
Nuclear Science & Engineering, 64, p. 465-479 (1977)

II. MONTE CARLO ANALYSIS AND CRITICALS PROGRAM PLANNING FOR SAFETY-RELATED CRITICALS (A2018)

A. Monte Carlo Analysis of Safety-Related Criticals (E. M. Gelbard)

Preliminary data reduction was begun for a Monte Carlo Analysis of the as-built reference Core. At present, a complete set of drawer masters and individual plate and material parameters has been collected and is being transcribed into input for the VIM Code.

B. Planning of Demo Safety Related Experiments (S. K. Bhattacharyya and L. LeSage)

The LMFBR Safety Related Critical Experiments were started on July 1, 1977. The various drawer masters necessary for the loading of the reference core, blanket and reflector were designed and all the drawers were fully preloaded (without the Pu fuel) before the actual start of loading in ZPR-9. The preloaded drawers were transferred to the ZPR-9 matrix after completion of the unloading of the Advanced Fuels Program core.

The physics measurements planned for the reference core were completed in early September and the subsequent measurements were initiated. The central test zone was sodium voided and the worth of this sodium voiding was determined. The fuel slump-out configuration was next achieved and the reactivity worth of this slumping-out was determined using conventional rod-drop and noise methods. The physics measurements were in progress in the fuel slump-out core at the end of the quarter.

Analysis of the experimental data is in progress. Some of the preliminary results will be presented here. The first experiment performed on the reference core was the approach-to-critical measurement. Starting from a fully preloaded configuration, fuel was added in steps in a radially symmetric manner to approach a critical configuration. At each step, subcritical multiplication data were accumulated using four in-core fission chambers, two out-of-core BF_3 ionization chambers and six reactor instruments. From each step, the critical mass was projected using the 1/C versus Fuel Mass (M), and the M/C versus M formulations (where C represents the count rate in the instrument in question). Figures 3 and 4 show typical results for the approach-to-ritical measurements. Figure 3 represents the M_f/C versus M_f plot for a centrally located ^{235}U fission chamber. A similar plot for a BF_3 ionization chamber located outside the radial reflector is shown in Fig. 4. As with earlier studies, the central detectors gave a good estimation of the critical mass from the early stages of the loading. After the fifth loading step, the central fission counters had to be removed from the central matrix locations to enable the loading of fuel in these locations. The subsequent loading steps were monitored by the external detectors. Figure 4 is an example of the results from these detectors. The erratic predictions at the final steps were attributed to the large changes made during these steps. The change from step 5 to 6 involved adding a significant amount of fuel at the center of the core, where the fission chambers had been located. The core radius was found to have been overestimated by the preanalysis and the change from step 6 to 7 involved the location of a large number of blanket drawers in

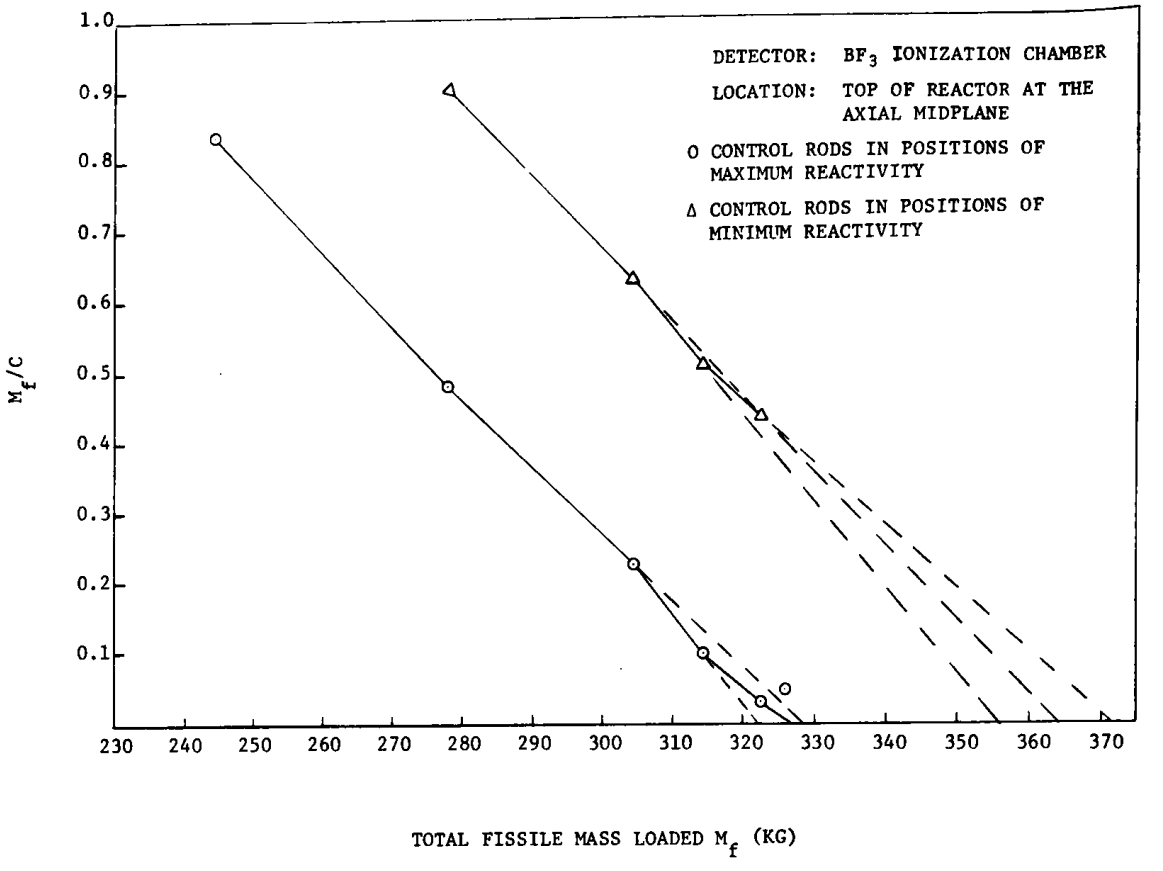

Fig. 3. Approach-to-Critical Plots from BF_3 Ionization Chamber Located Outside the Radial Reflector. ANL Neg. No. 116-77-938.

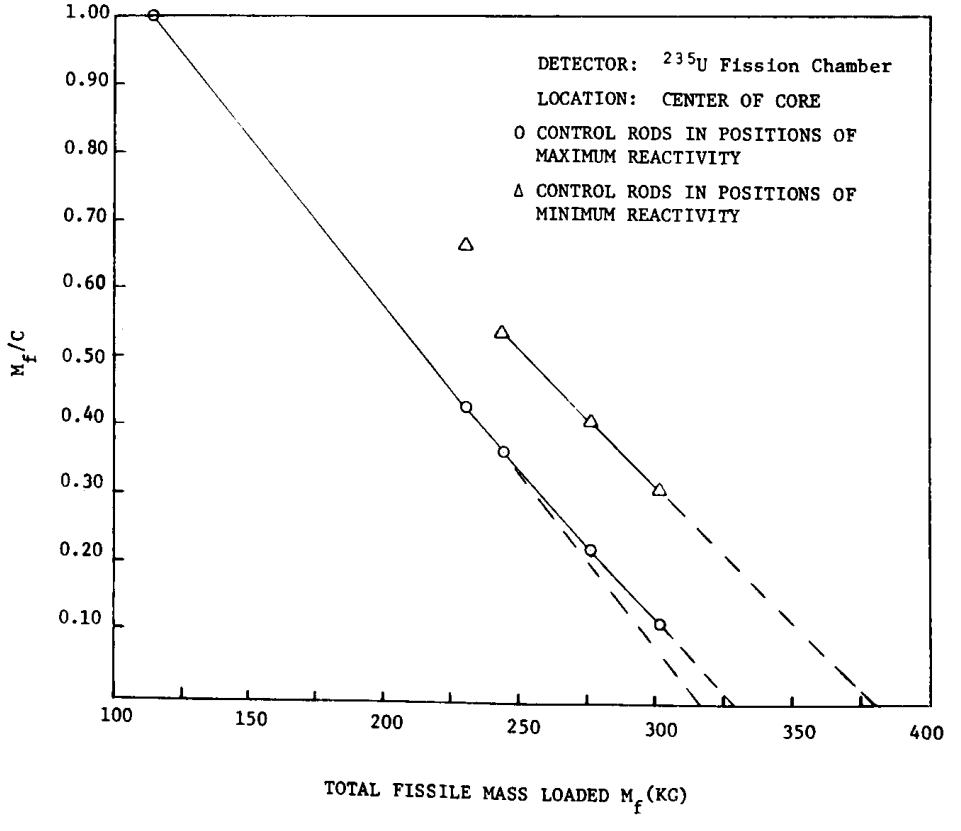

Fig. 4. Approach-to-Critical Plots from ^{235}U Fission Chamber Located at Core Center ANL Neg. No. 116-77-939.

preloaded core drawer locations. However at these stages of the approach-to-critical, noise measurements and rod-drop measurements provided a reasonably reliable measure of subcriticality. At each stage, the measurement was made both with the control rods in their positions of maximum and positions of minimum reactivity to provide a measure of the available control. The final critical configuration was achieved on August 8, 1977. It had a fissile loading of 332.58 ± 2.0 kg with a measured excess reactivity of 85 Ih (0.27$). Figure 5 shows a core map of the reference configuration with all the operational control rods and thermocouple positions indicated. Various operational measurements were performed to establish the worths of the operational control rods, the temperature coefficient of the assembly and a worth versus position calibration for two of the dual purpose control rods.

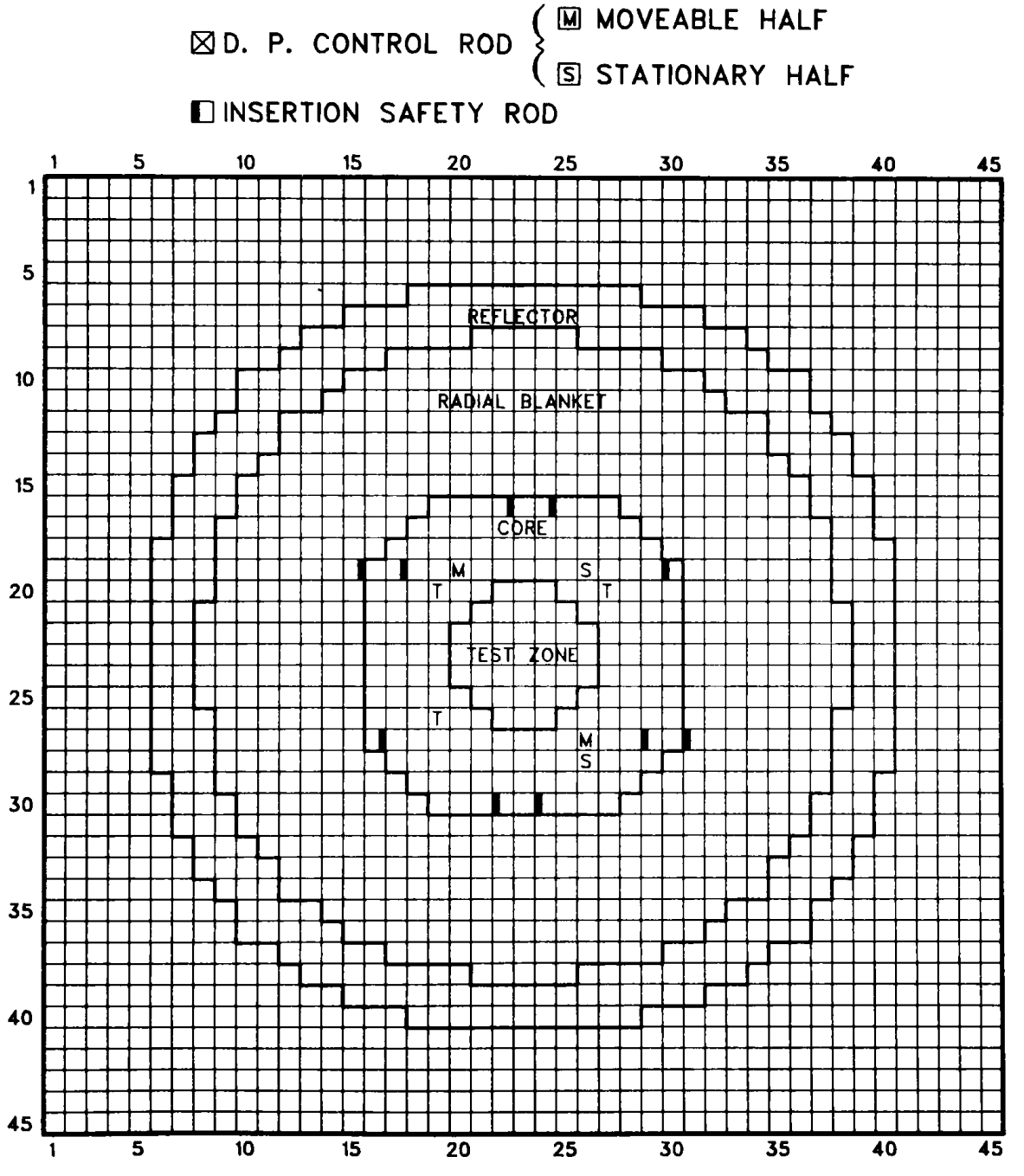

Fig. 5. Core Map of the Reference Configuration of the LMFBR Safety Related Critical Experiments Program ANL Neg. No. 116-77-941.

Preliminary results are available for the β_{eff} measurement in the reference core. According to noise theory, β_{eff}^2 can be expressed in terms of measurable parameters and a calculated Diven factor D as

$$3/8\ D/\beta_{eff}^2 = F\ \$\ \frac{\tau\sigma^2}{[4\$/(1+\$)^2]}$$

where F is the average fission rate in the assembly, \$ gives the reactivity of the configuration in question, τ is the flux sampling interval, and σ^2 is the joint-local-variance.

Table III gives the numerical values of the parameters in the expression. The Diven factor, D, has not yet been computed for the reference core, but it is not expected to be very different from the value computed for the GCFR Phase I assembly. The experimental value of β_{eff} was found to be 0.003728 ± 2.5% which gives a C/E value of 0.86. This is slightly lower than earlier experience with the GCFR critical assembly in which a C/E value of 0.90 was obtained. The experimental value reported here should be treated as preliminary at this point.

TABLE III. Parameters Used in the Calculation of β_{eff}

Parameter	Numerical Value
$\frac{\tau\sigma^2}{4\$/(1+\$)^2}$	0.700×10^{-5} (%1%)
F	1.6577×10^{11} (±4%)
D	0.929[a]
\$	0.2160×10^{-1} (±1.5%)

[a] Calculated value for GCFR Phase I assembly.

THREE-DIMENSIONAL CODE DEVELOPMENT FOR CORE THERMAL HYDRAULIC ANALYSIS OF LMFBR ACCIDENT UNDER NATURAL CONVECTION CONDITIONS

A. Numerical Simulation of the Thermal Hydraulics of a 19-Pin LMFBR Fuel Assembly in a Hexagonal Duct (W. T. Sha, H. M. Domanus and R. C. Schmitt)

To realistically simulate the velocity and temperature distributions in an LMFBR fuel assembly requires some modifications of the continuum approach. These modifications are to introduce distributed resistance and porosity[9,10] to account for the presence of fuel rods.

The COMMIX-1 computer code is used to compute the temperature and velocity distributions in a fuel assembly. These results are then compared with experimental data obtained at Oak Ridge National Laboratory in 1973.[11] The LMFBR fuel assembly contains 19 rods arranged in a hexagonal duct and is referred to as FFM bundle 2A (Fuel Failure Mockup). The test section used for the experiments is shown in Fig. 6. The current analysis consists of a 0.3048 meter entrance region followed by a 0.5334 meter heated length and a 0.1524 meter exit region. The overall axial length is partitioned into 13 equal division as shown in Fig. 7. The z-axis is aligned with the axial flow direction. Gravity is in the -z direction. The partitioning of transverse planes is shown in Fig. 8. The quasi-continuum formulation is used to analyze the fuel pins.

1. Hex Fuel Assembly Problem Statement

Sodium at 309.4°C is entering the bundle at the bottom uniformly at a velocity of 0.127 meter/sec. As the sodium folows through the duct, it is non-uniformly heated. The radial power density distributions is shown in Fig. 8. The total amount of heat added to the sodium over the heated section is 10.3 KW. Since the COMMIX-1 code is a transient code, a suitable initial condition was chosen and a transient analysis performed until steady state was reached. In order to speed the convergence, an educated guess of the initial condition is chosen. This guess was taken as the axial 1-D solution, assuming no variation over a given axial plane.

2. Hex Fuel Assembly Results

The steady-state velocity distribution is shown in Fig. 9 through 21. Each is a projection of the velocity vectors in axial planes along the hexagonal duct. After the flow enters the duct uniformly, it spreads toward the walls due to the relatively high resistance in the central region and low resistance near the duct walls. Towards the end of the entrance region (Fig. 12), the first effects of the nonuniformly heated rods are seen. This is due to an unbalanced up-draft set up by the pins with relatively high power density. This skewed up-draft continues to the end of the heated region where the flow begins to return toward an isothermal flow pattern. Figures 22 through 27 show this skewed up-draft action with the axial velocity components shown as a surface across the duct along the axial length. The temperature distributions over a duct cross-section at the axial positions are shown in Figs. 28 through 33. A comparison between measured and COMMIX-1 calculated outlet temperatures is shown in Fig. 34. As can be seen, agreement is excellent.

Only cartesian coordinates can be handled by the present version of plot routine (Figures 22-33); modification is planned to account for hex geometry.

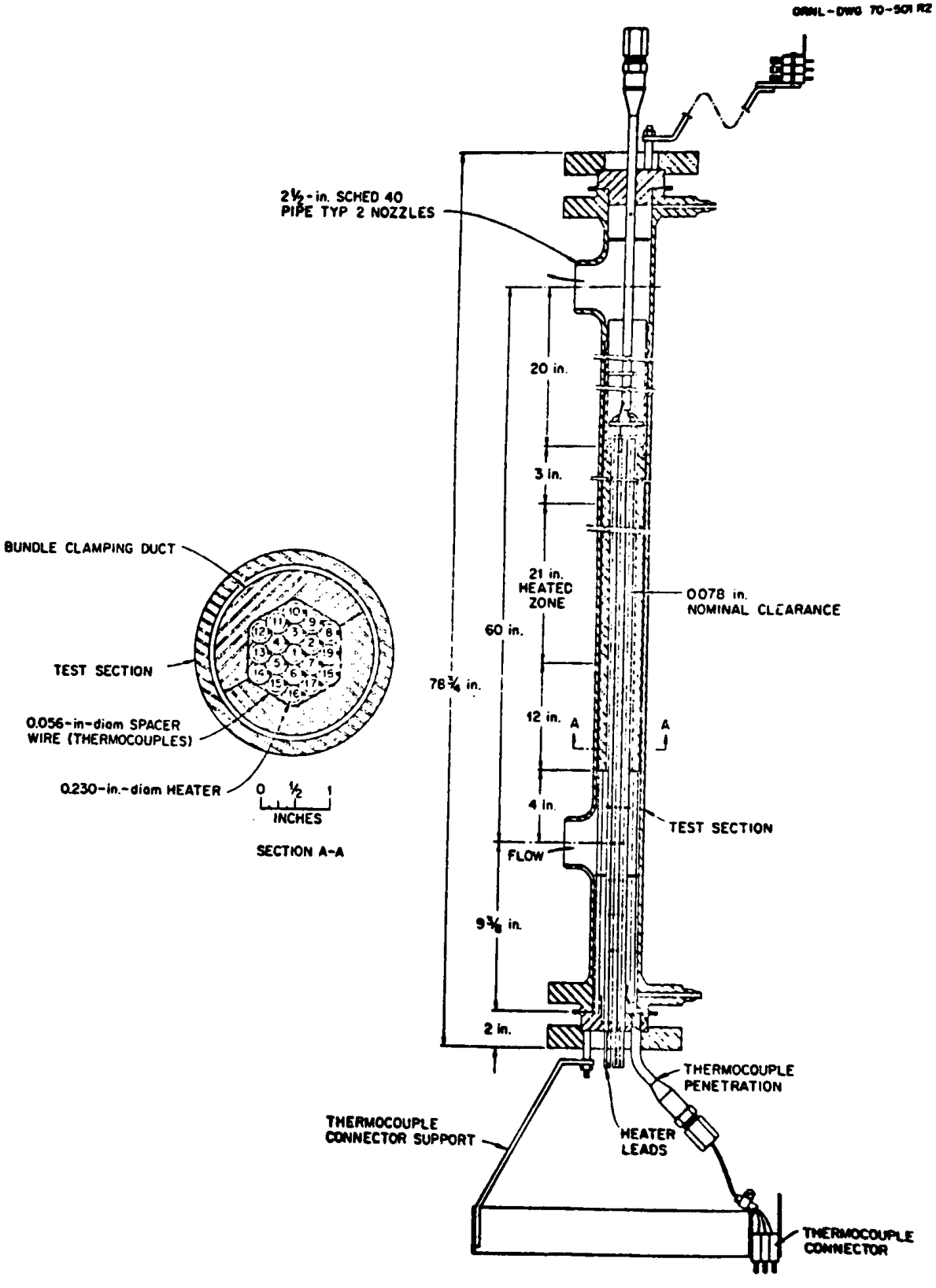

Fig. 6. LMFBR - FFM - Test Section Assembly for Bundle 2A ANL Neg. No. 116-77-935.

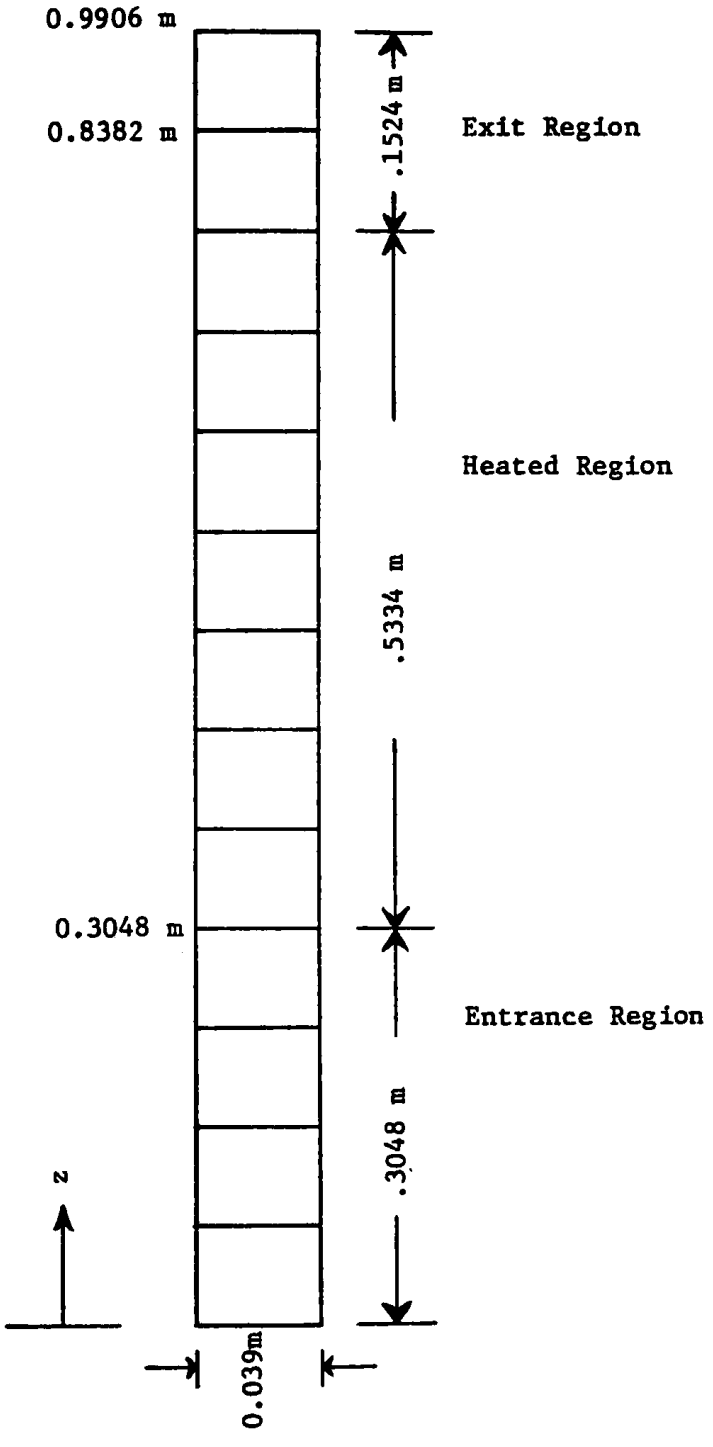

Fig. 7. Axial Partitioning Used in LMFBR Fuel Pin Bundle Analysis ANL Neg. No. 116-77-922.

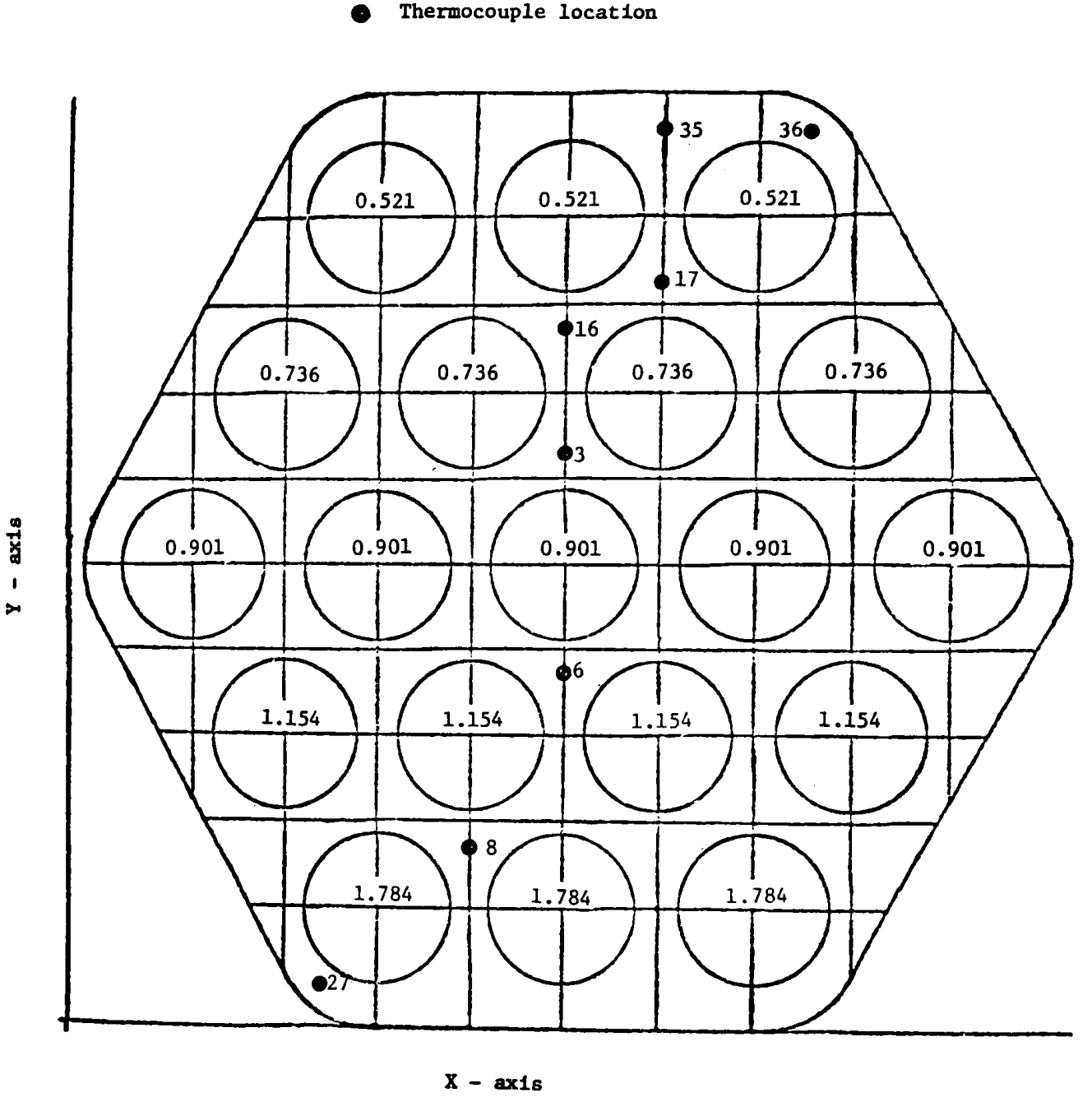

Fig. 8. Normalized Radial Pin Power Density Distribution
ANL Neg. No. 116-77-936

VELOCITY DISTRIBUTION

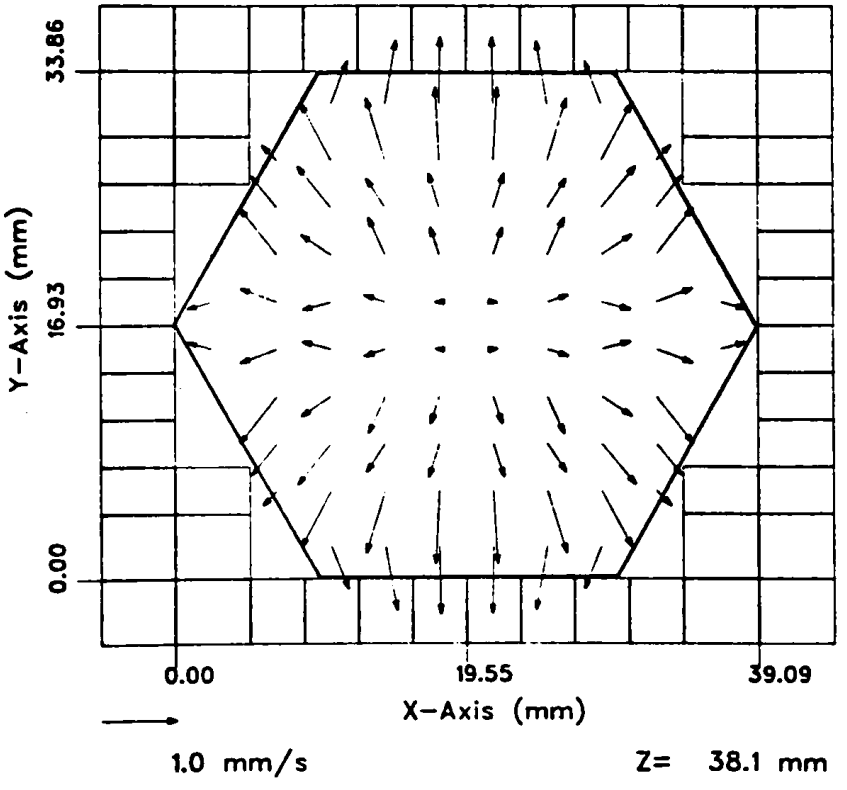

Fig. 9

Steady Velocity Distribution at Z = 0.0381 m from Inlet (Entrance Region) ANL Neg. No. 116-77-928.

VELOCITY DISTRIBUTION

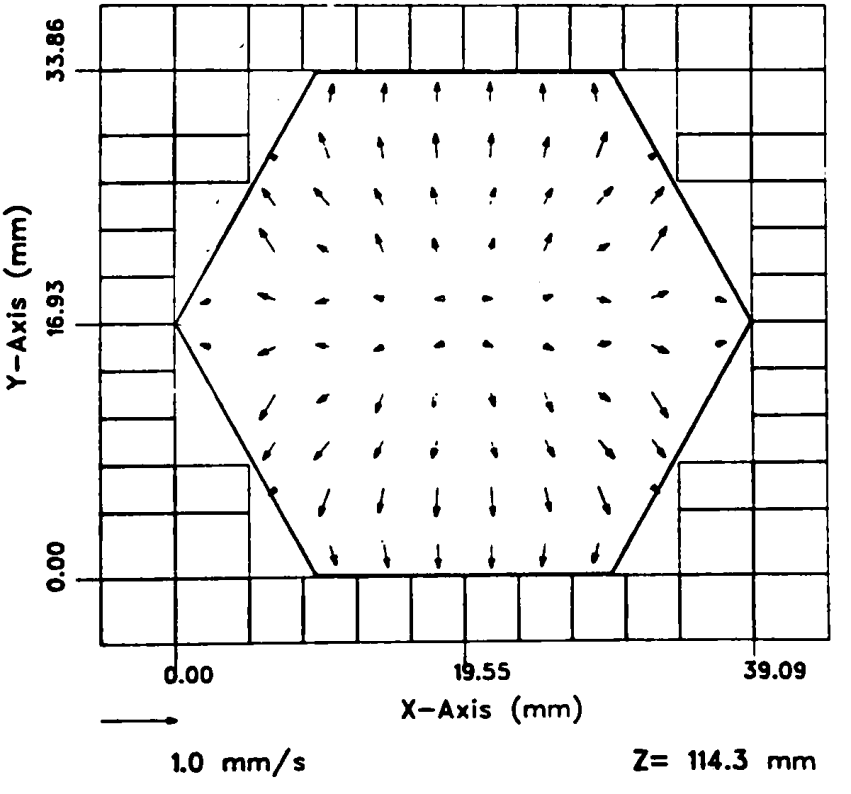

Fig. 10.

Steady Velocity Distribution at Z = 0.1143 m from Inlet (Entrance Region) ANL Neg. No. 116-77-955.

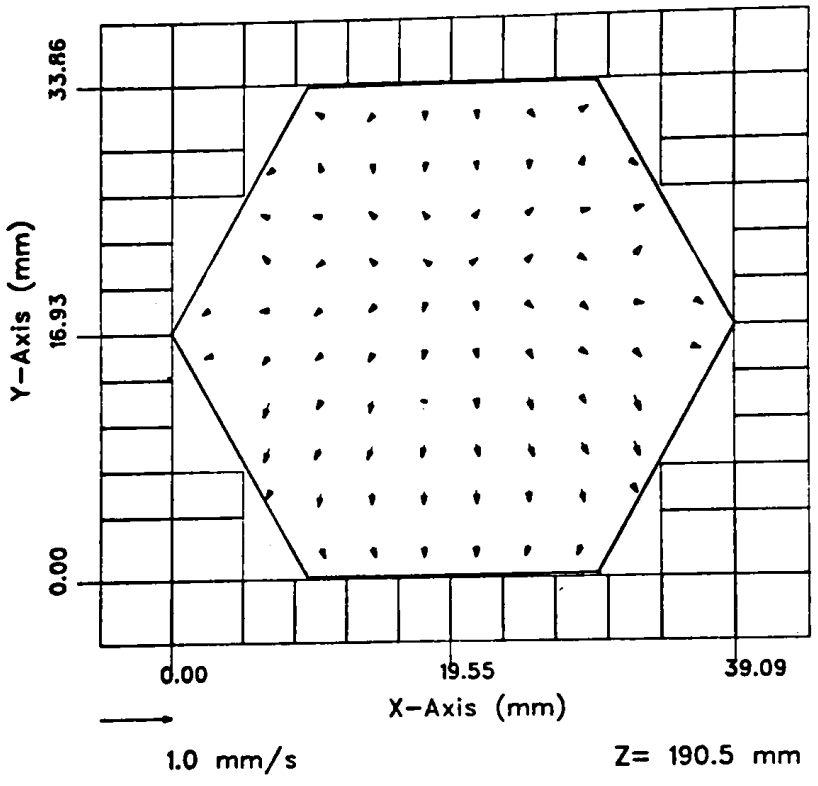

Fig. 11.

Steady Velocity Distribution at Z = 0.1905 m from Inlet (Entrance Region) ANL Neg. No. 116-77-927.

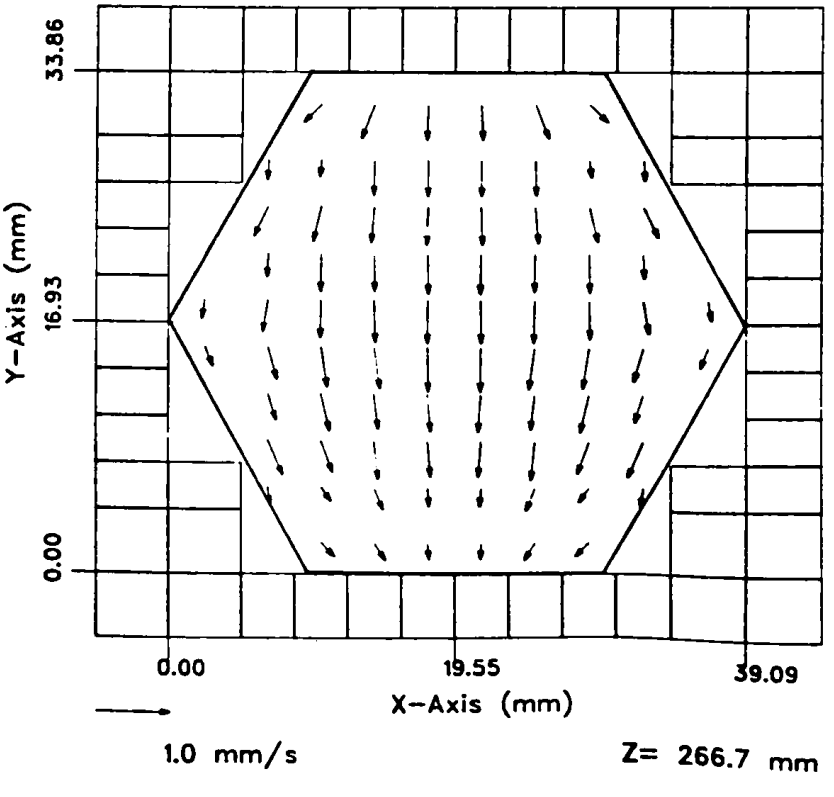

Fig. 12.

Steady Velocity Distribution at Z = 0.2667 m from Inlet (Entrance Region) ANL Neg. No. 116-77-951.

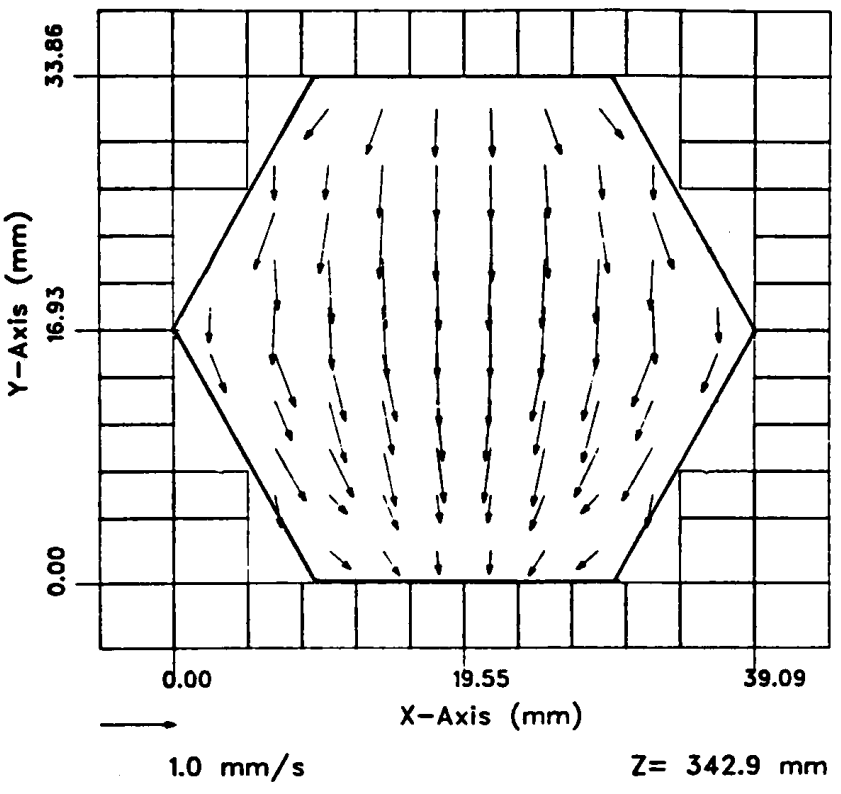

Fig. 13.

Steady Velocity Distribution at Z = 0.3429 m from Inlet (Heated Region) ANL Neg. No. 116-77-952.

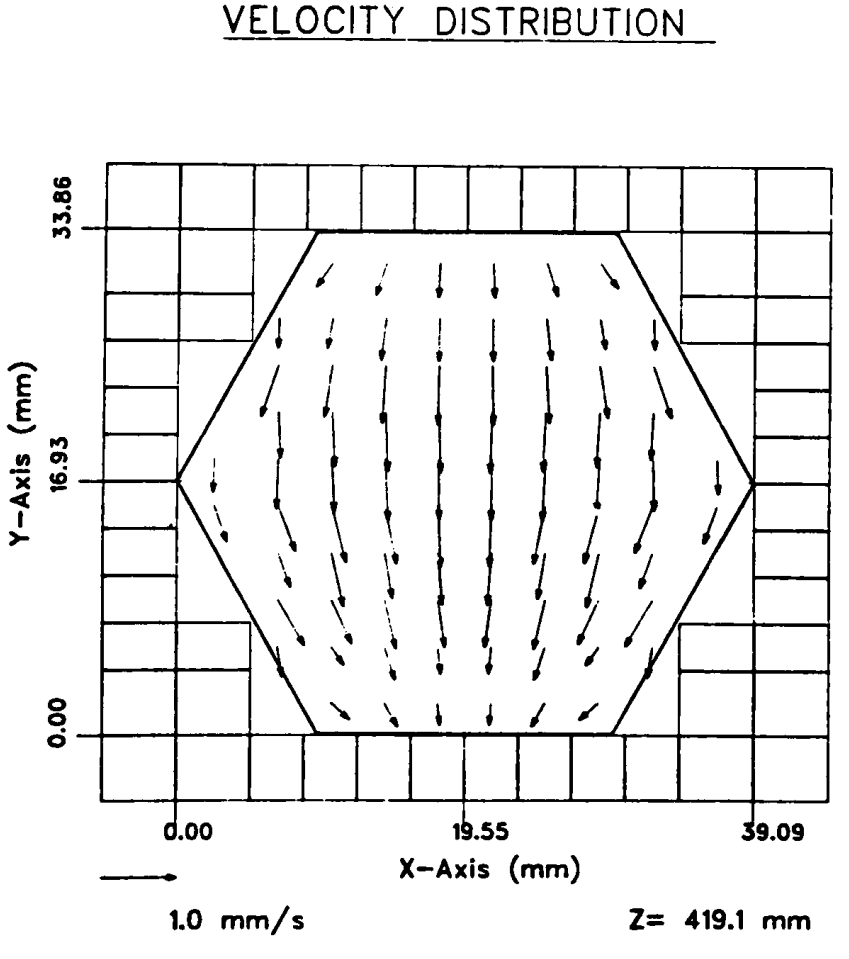

Fig. 14.

Steady Velocity Distribution at Z = 0.4191 m from Inlet (Heated Region) ANL Neg. No. 116-77-931.

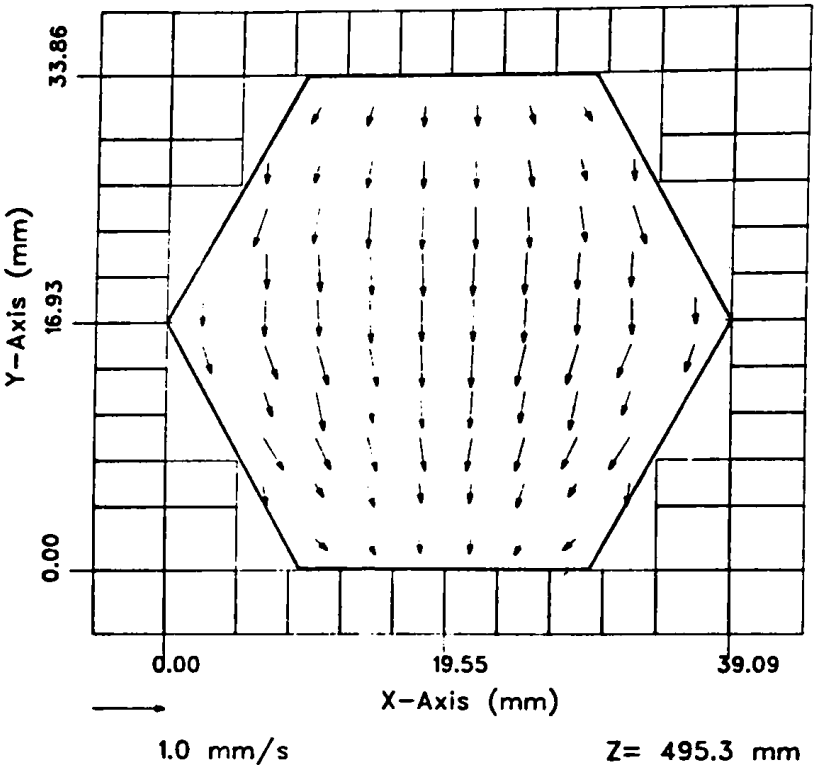

Fig. 15.

Steady Velocity Distribution at Z = 0.4953 m from Inlet (Heated Region) ANL Neg. No. 116-77-930.

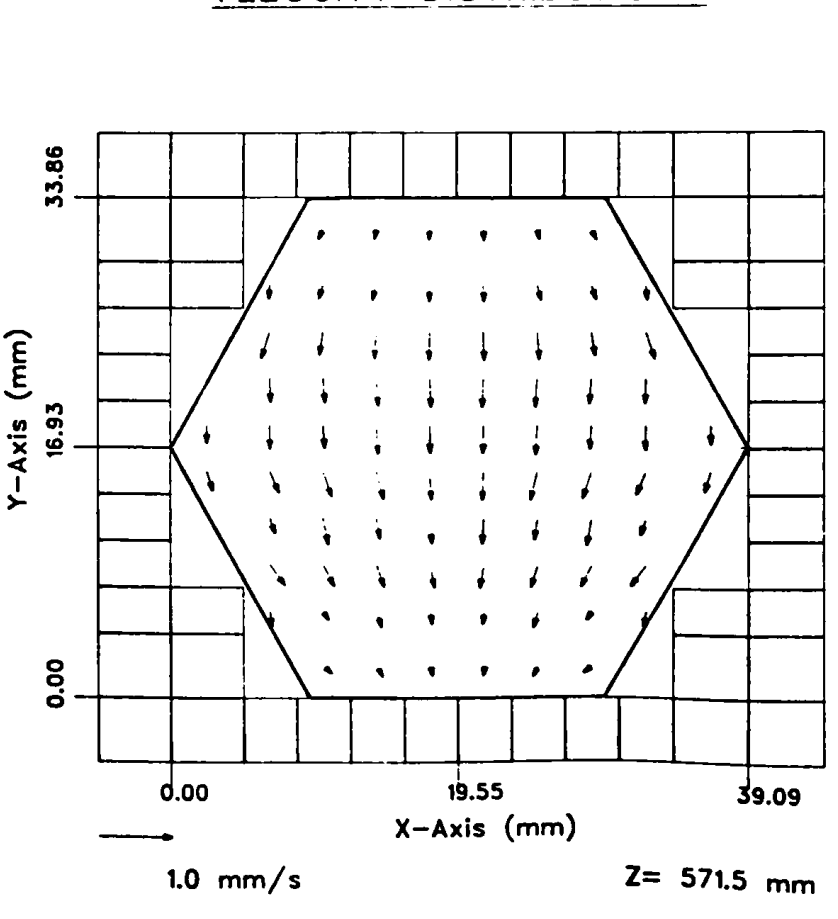

Fig. 16.

Steady Velocity Distribution at Z = 0.5715 m from Inlet (Heated Region) ANL Neg. No. 116-77-953.

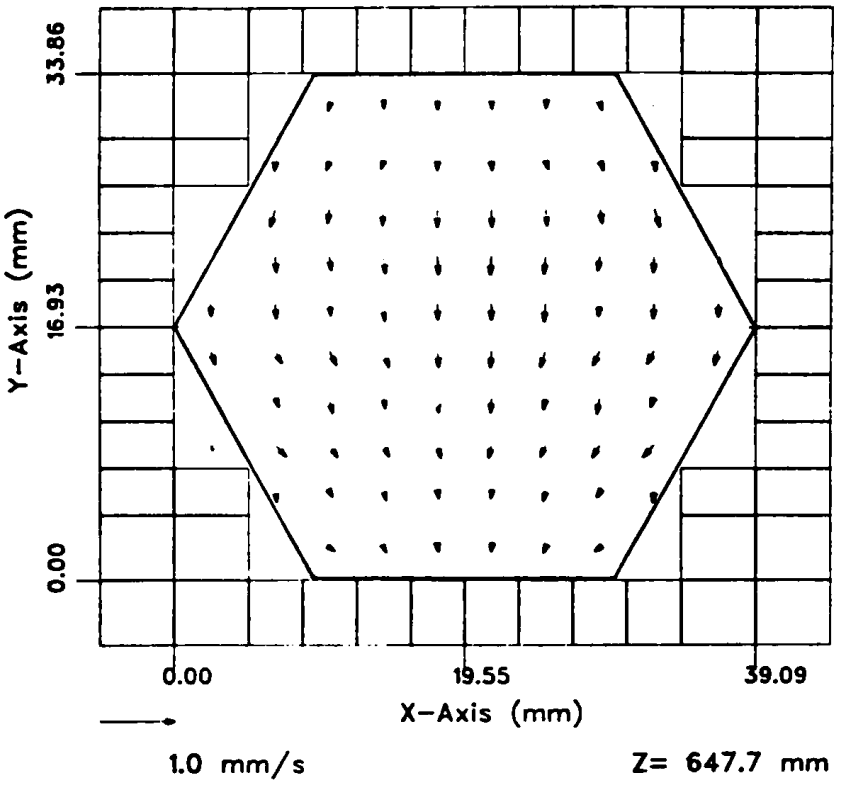

Fig. 17.

Steady Velocity Distribution at Z = 0.6477 m from Inlet (Heated Region) ANL Neg. No. 116-77-954.

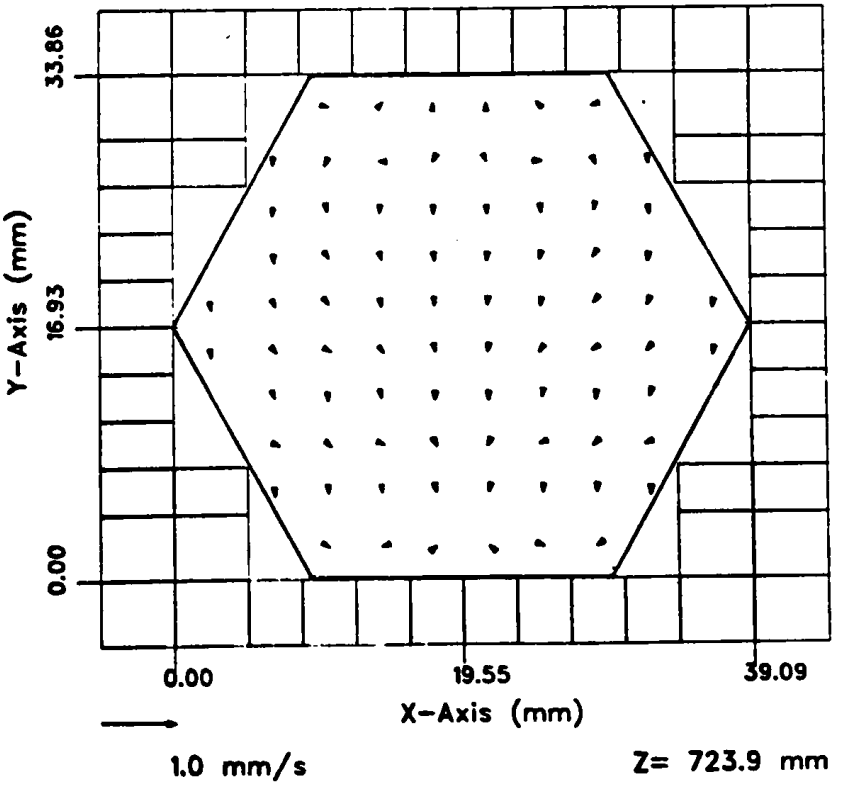

Fig. 18.

Steady Velocity Distribution at Z = 0.7239 m from Inlet (Heated Region) ANL Neg. No. 116-77-932.

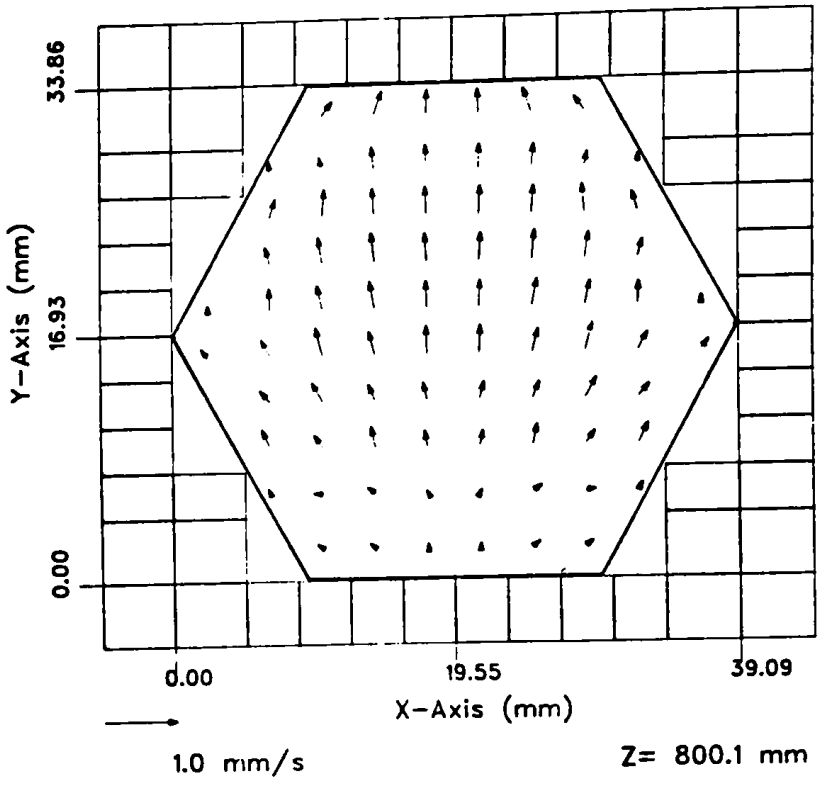

Fig. 19.

Steady Velocity Distribution at Z = 0.8001 m from Inlet (Heated Region) ANL Neg. No. 116-77-933.

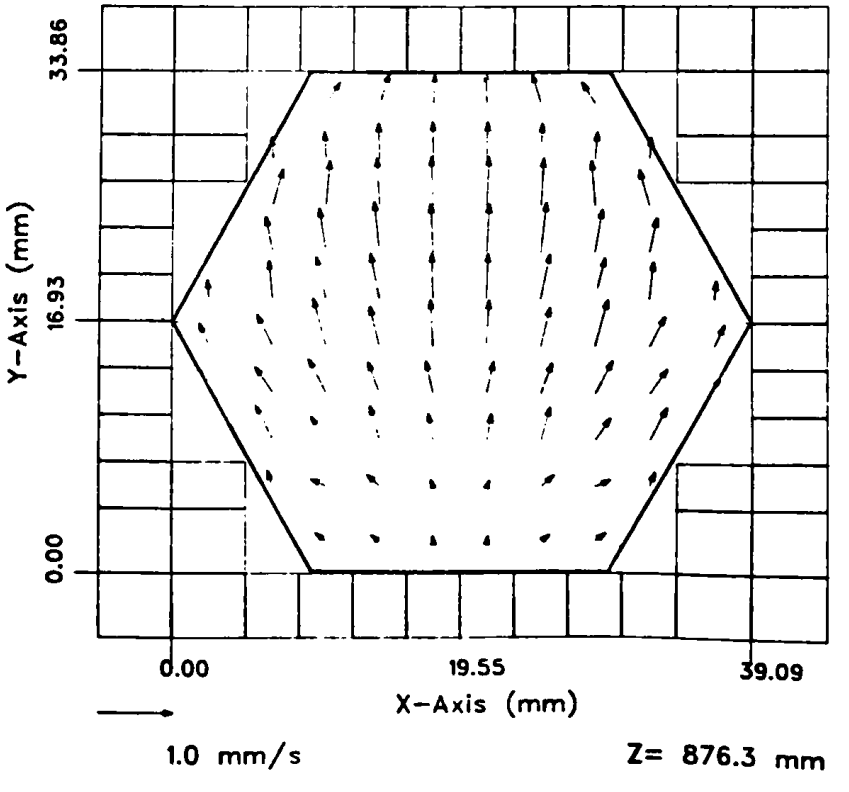

Fig. 20.

Steady Velocity Distribution at Z = 0.8763 m from Inlet (Exit Region) ANL Neg. No. 116-77-929.

VELOCITY DISTRIBUTION

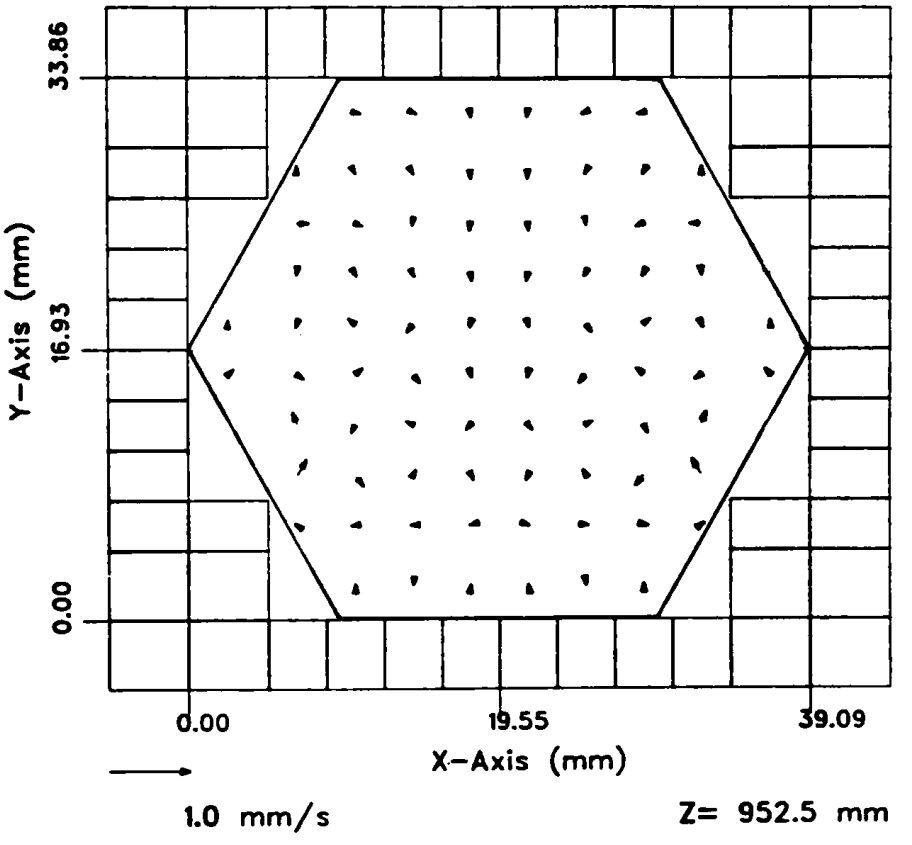

Fig. 21.
Steady Velocity Distribution at Z = 0.9525 m from Inlet (Exit Region) ANL Neg. No. 116-77-942.

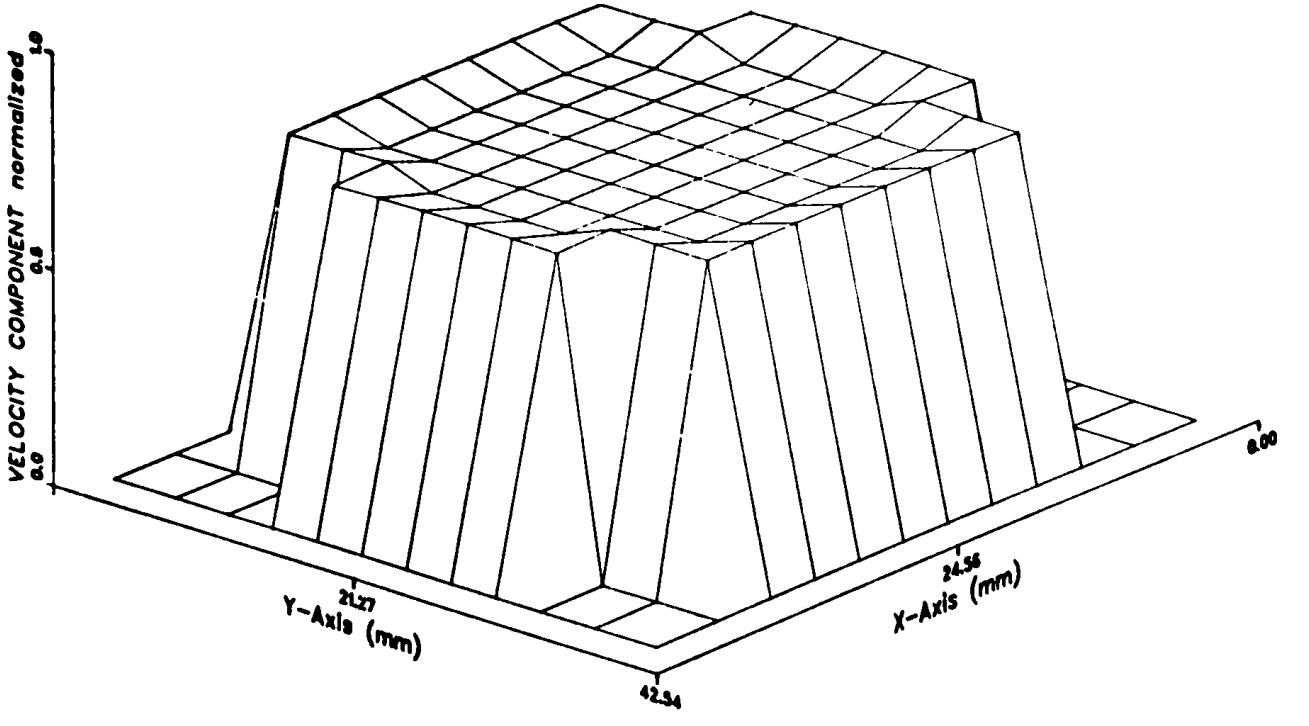

Fig. 22. Steady Axial Velocity Distribution at Z = 0.0381 m from Inlet (Entrance Region) ANL Neg. No. 116-77-943.

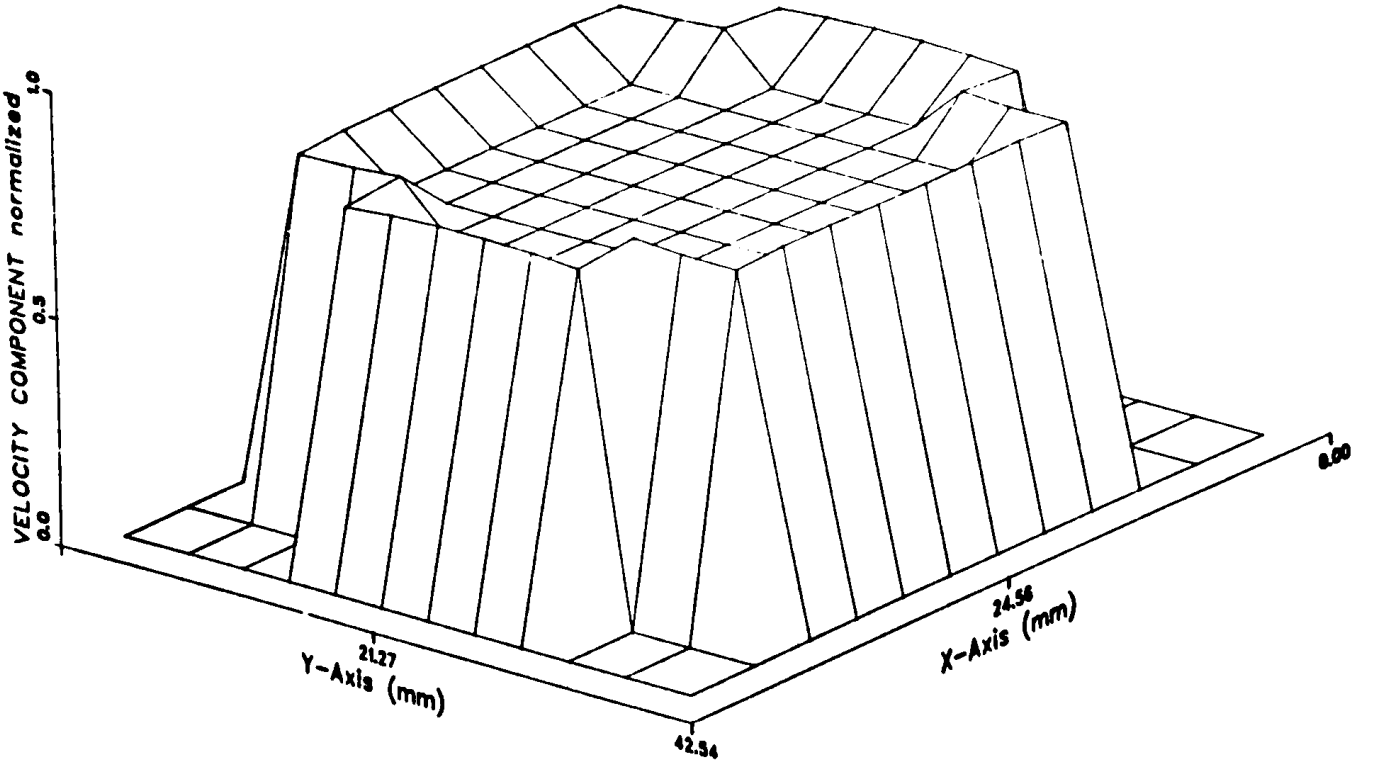

Fig. 23. Steady Axial Velocity Distribution at Z = 0.1143 m from Inlet (Entrance Region) ANL Neg. No. 116-77-923 .

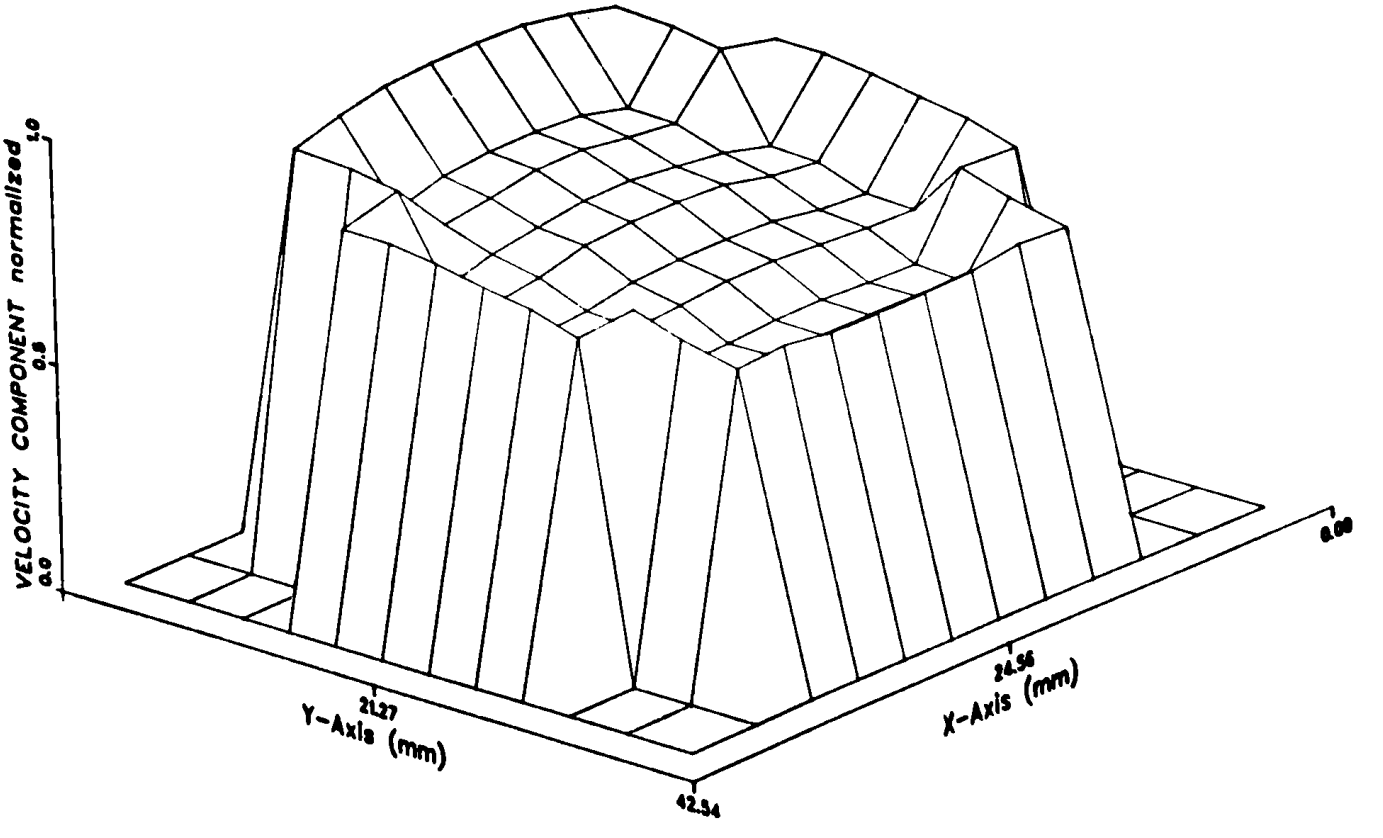

Fig. 24. Steady Axial Velcoity Distribution at Z = 0.5715 m from Inlet (Heated Region) ANL Neg. No. 116-77-924 .

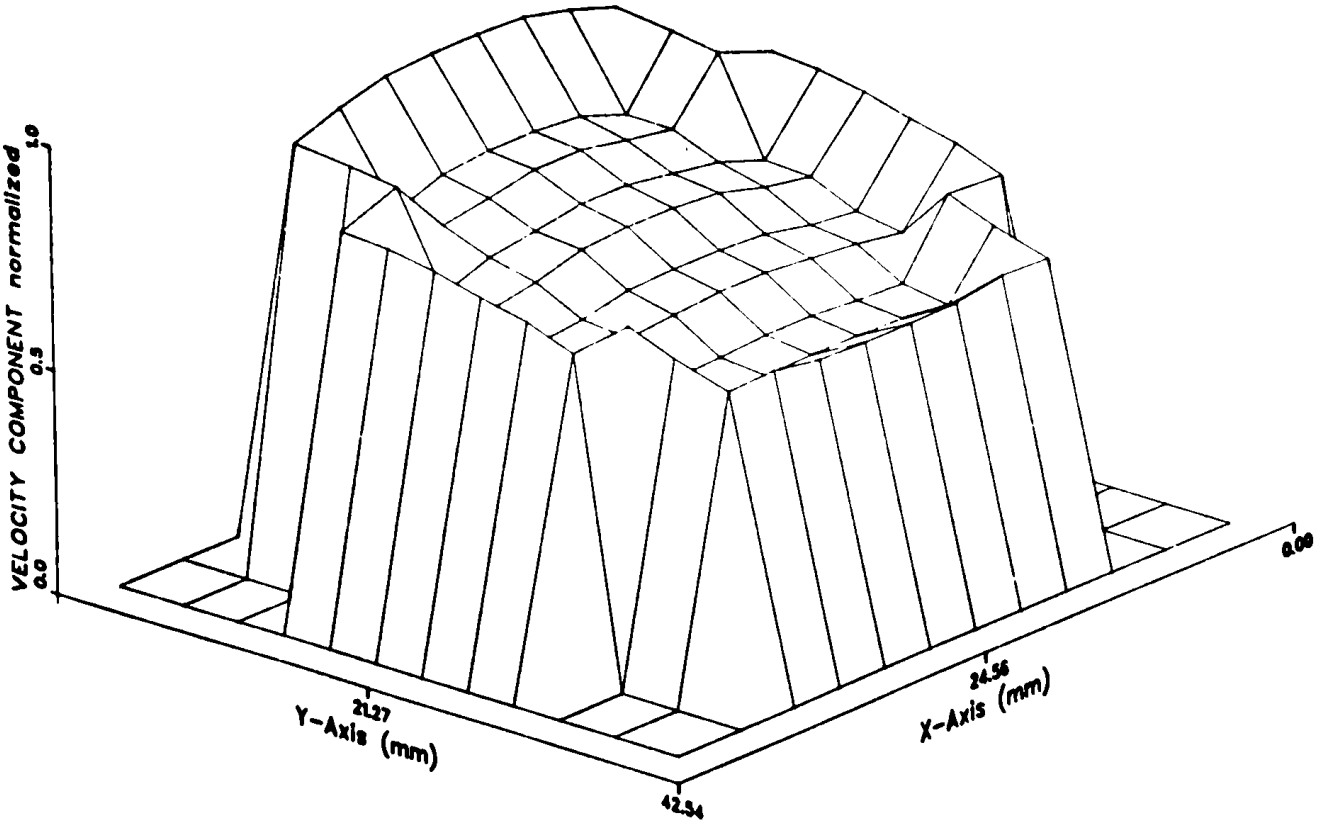

Fig. 25. Steady Axial Velocity Distribution at Z = 0.8001 m from Inlet (Heated Region) ANL Neg. No. 116-77-950.

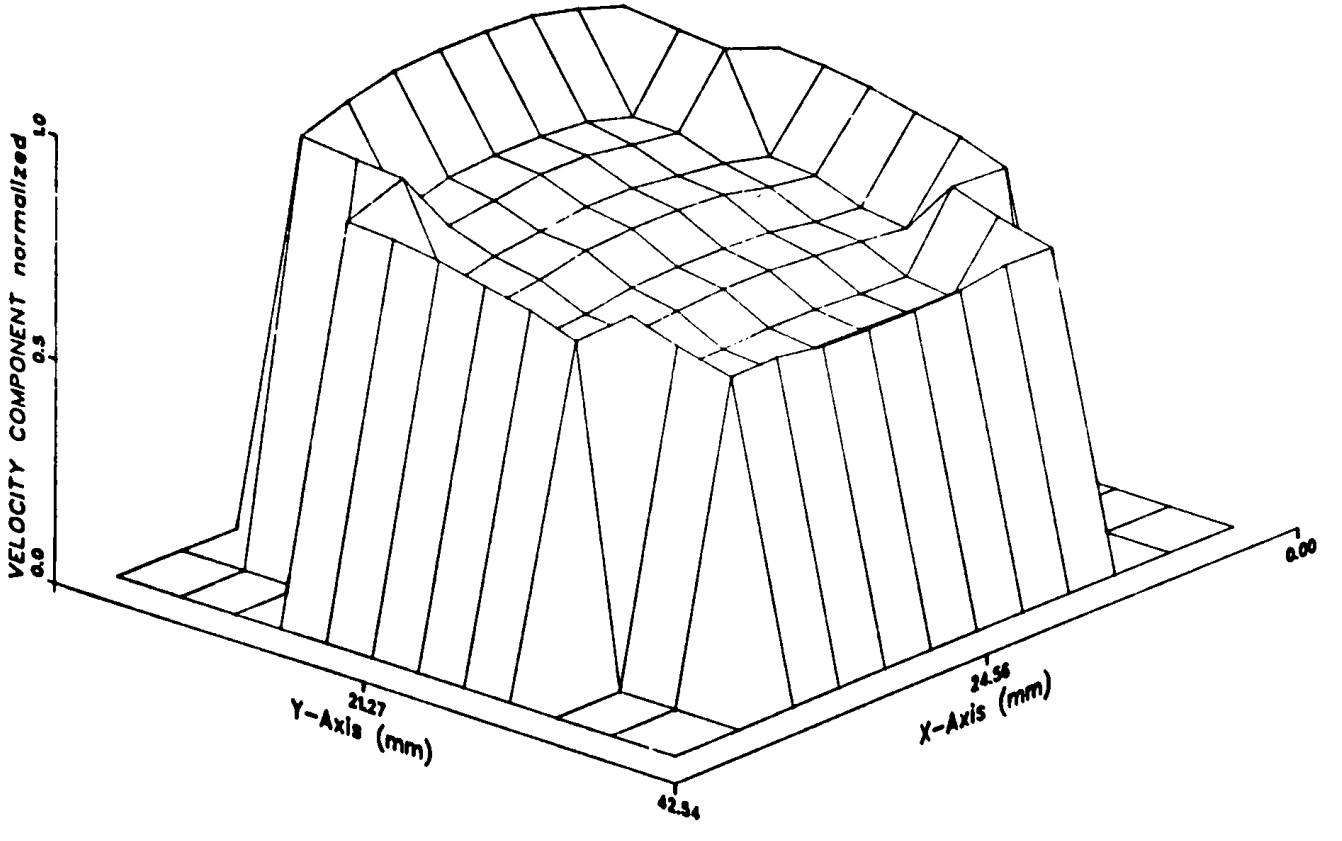

Fig. 26. Steady Axial Velocity Distribution at Z = 0.8763 m from Inlet (Exit Region) ANL Neg. No. 116-77-925.

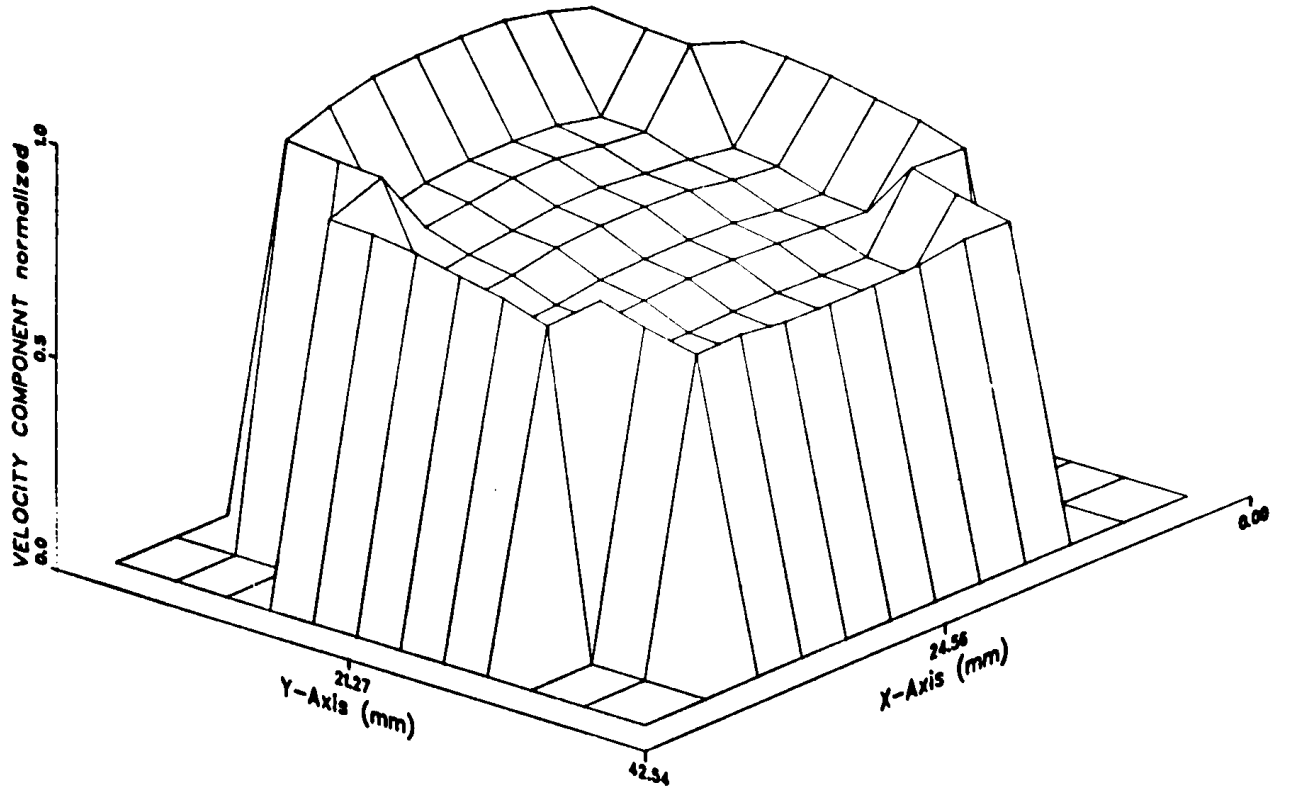

Fig. 27. Steady Axial Velocity Distribution at Z = 0.9525 m from Inlet (Exit Region) ANL Neg. No. 116-77-945.

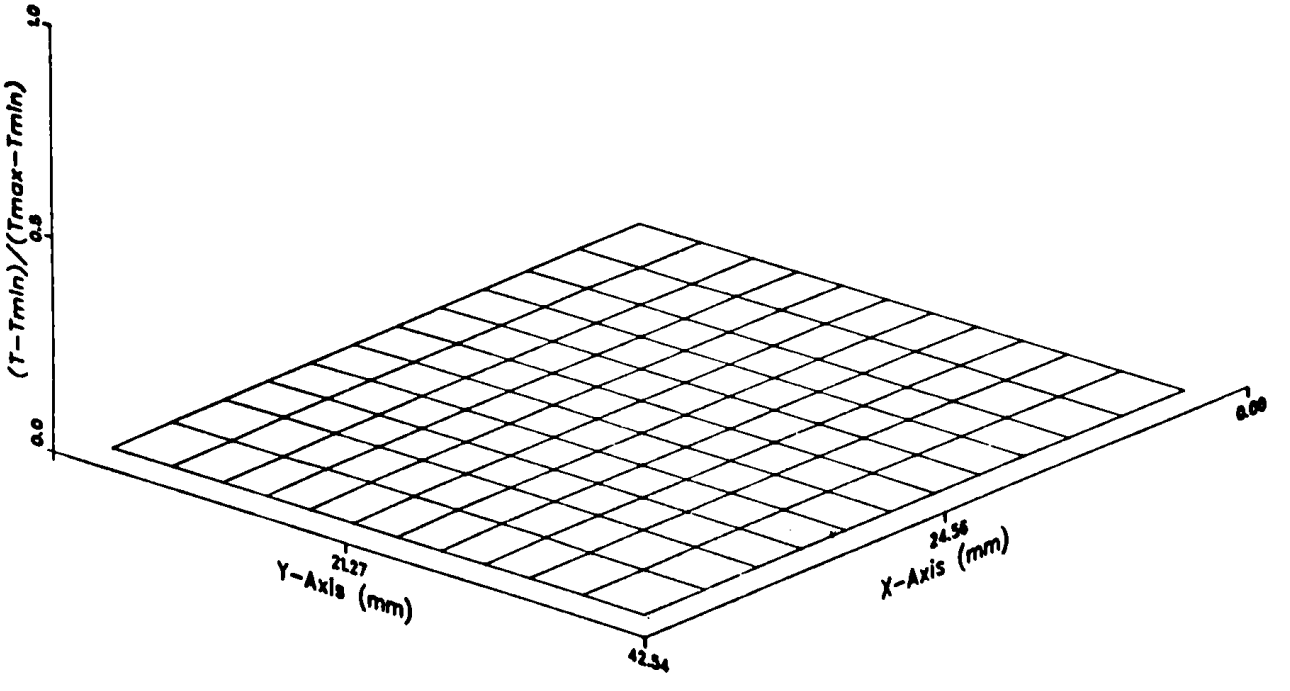

Fig. 28. Steady Temperature Distirbution at Z = 0.2667 m from Inlet (Entrance Region) ANL Neg. No. 116-77-947.

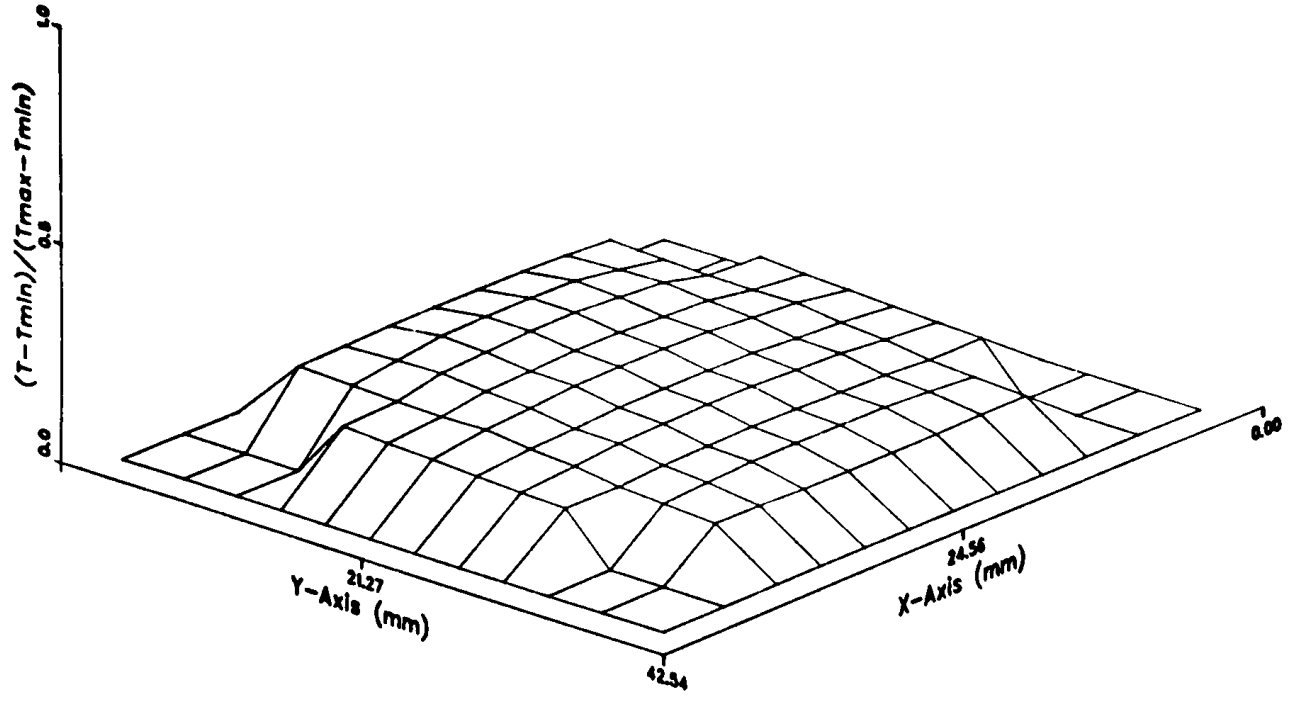

Fig. 29. Steady Temperature Distribution at Z = 0.3429 m from Inlet (Heated Region) ANL Neg. No. 116-77-946.

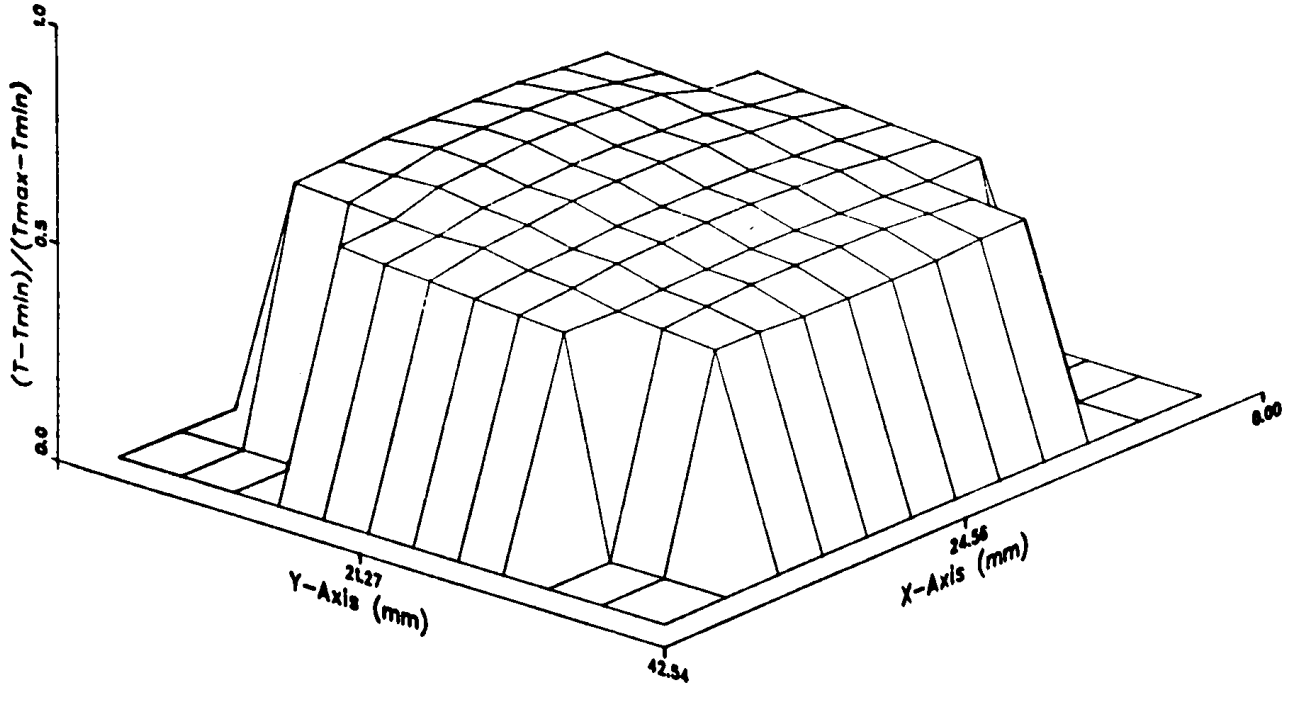

Fig. 30. Steady Temperature Distribution at Z = 0.5715 m from Inlet (Heated Region) ANL Neg. No. 116-77-949.

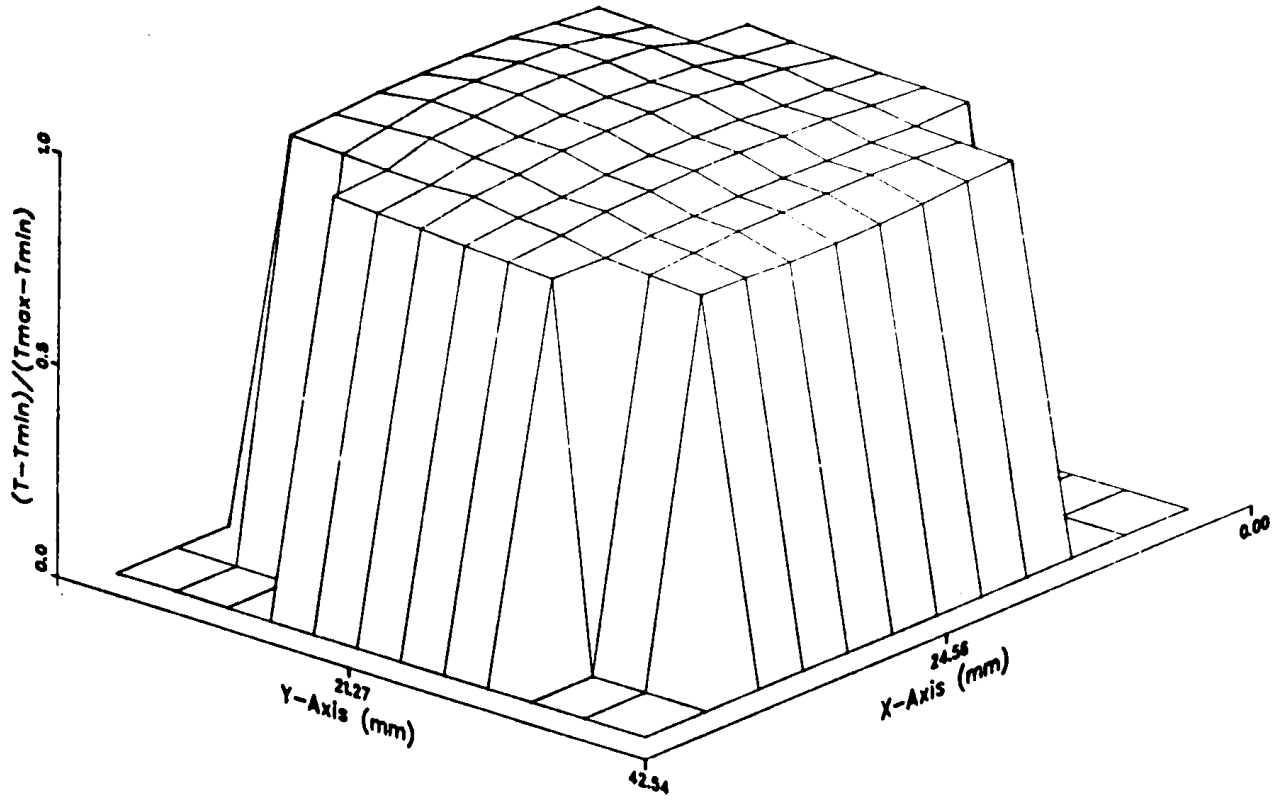

Fig. 31. Steady Temperature Distribution at Z = 0.8001 m from Inlet (Heated Region) ANL Neg. No. 116-77-948.

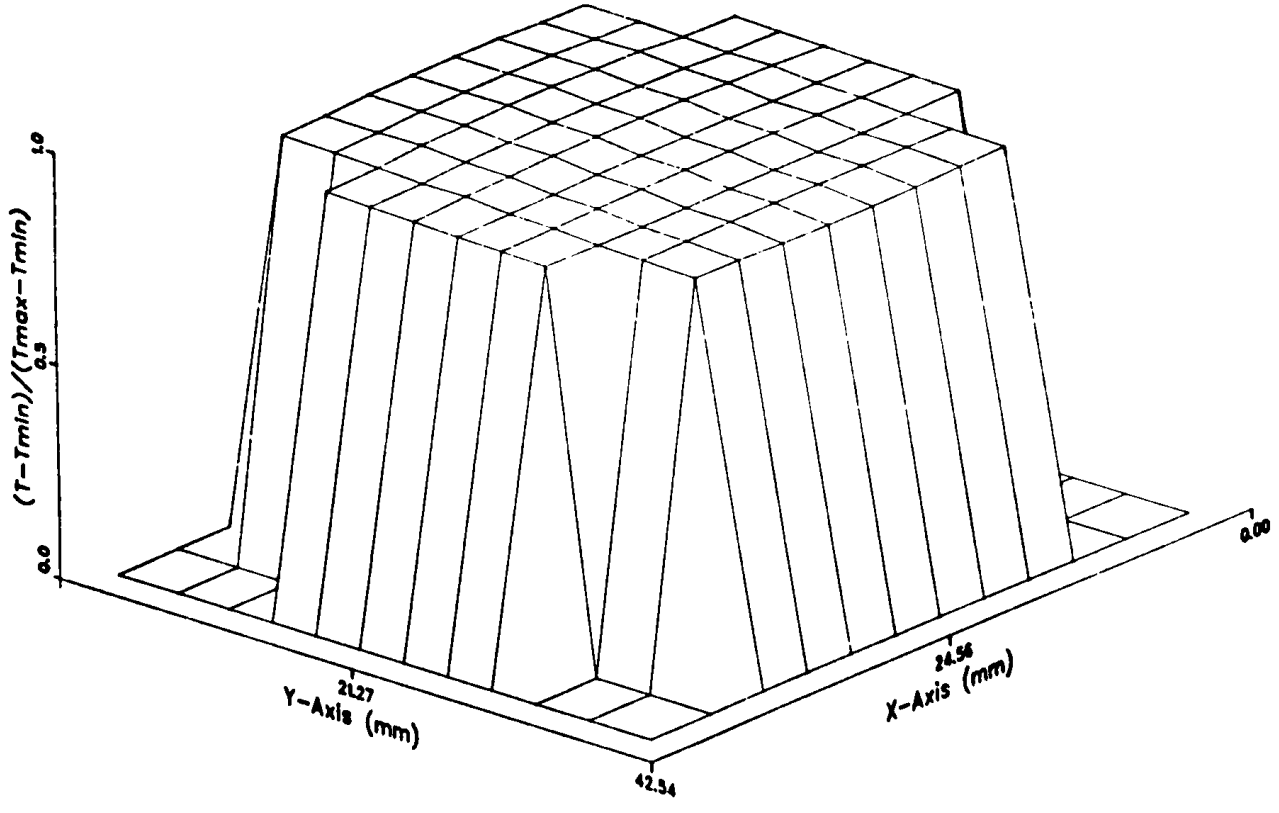

Fig. 32. Steady Temperature Distribution at Z = 0.8763 m from Inlet (Exit Region) ANL Neg. No. 116-77-944.

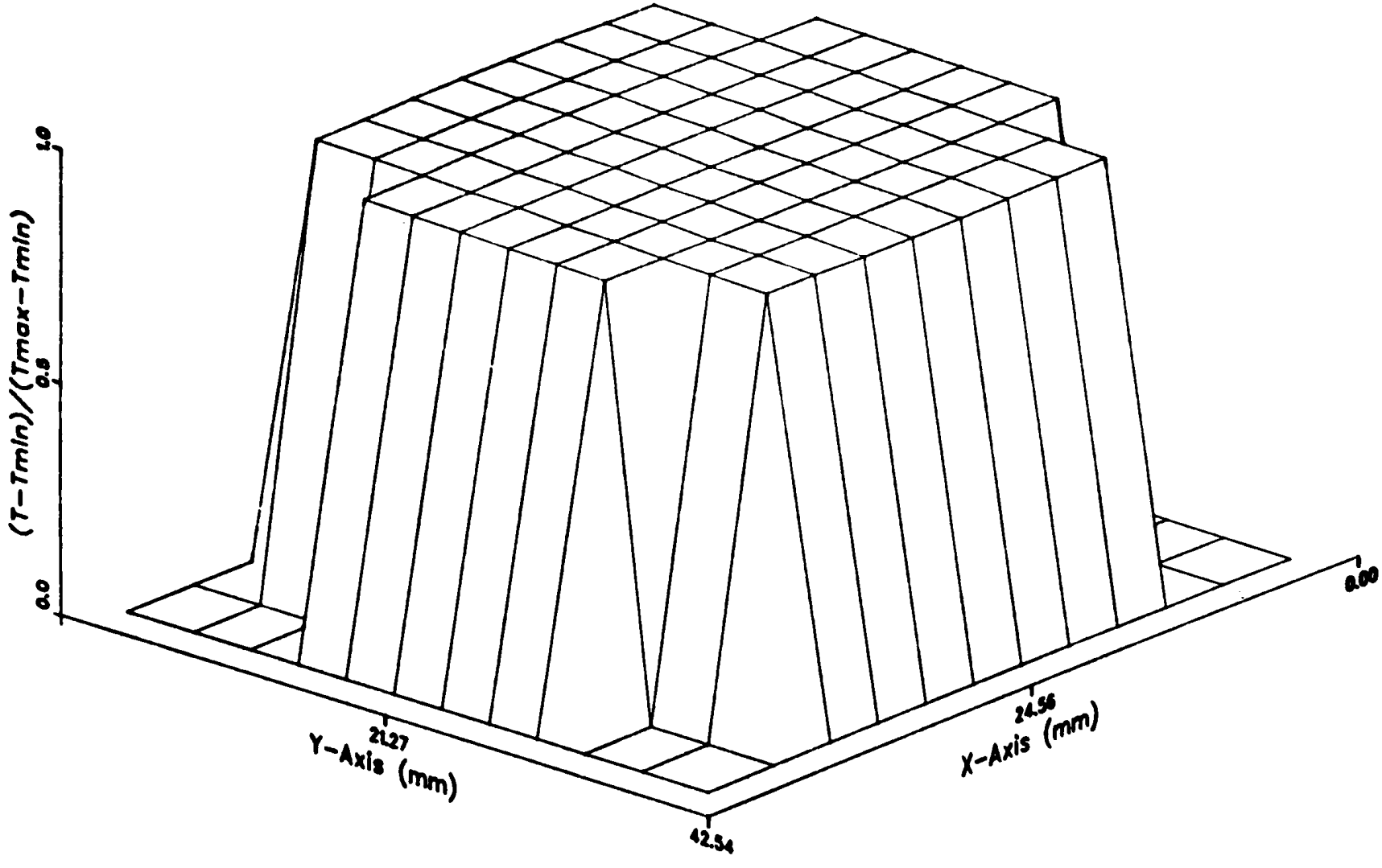

Fig. 33. Steady Temperature Distribution at Z = 0.9525 m from Inlet (Exit Region) ANL Neg. No. 116-77-934.

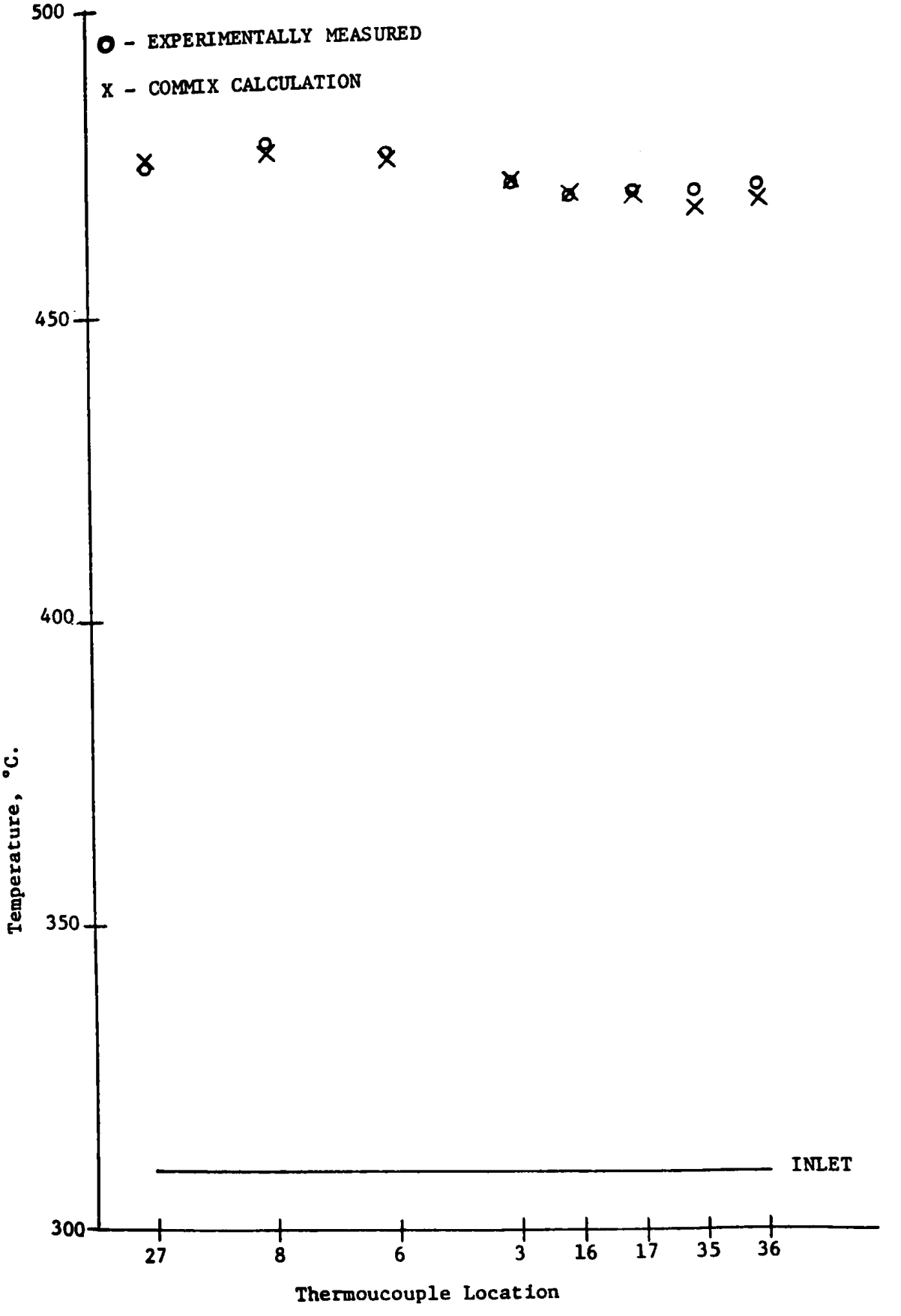

Fig. 34. COMMIX-1 vs. Experiment: Outlet Temperature Distribution ANL Neg. No. 116-77-926.

References

1. Physics of Reactor Safety: Quarterly Report, July-September 1976, Argonne National Laboratory Report ANL-77-9 (December 1976) p. 11.

2. Physics of Reactor Safety: Quarterly Report, April-June 1977, Argonne National Laboratory Report ANL-77-69, p. 15.

3. Physics of Reactor Safety, Quarterly Reprt, July-September 1976, Argonne National Laboratory, ANL-77-9, p. 11.

4. J. W. Wald and I. S. Levy, LMFBR Fuel Pin Cladding Transient Performance Capabilities: An Analysis of FCTT Data, BNWL-2041 (March 1976).

5. C. W. Hunter, G. D. Johnson and R. L. Fish, Mechanical Properties during Simulated Overpower Transients of Fast Reactor Cladding Irradiated from 700-1000°F, HEDL-TME 75-28, Hanford Engineering Development Laboratory (June 1975).

6. J. L. Straalsund, R. L. Fish, and G. D. Johnson, Correlation of Transient-Test Data with Convetional Mechanical Properties, Nucl. Tech., 25, p. 531 (1975).

7. G. D. Johnson, C. W. Hunter and J. E. Hanson, Fuel Cladding Mechanical Properties for Transient Analysis, Internal Meeting on Fast Reactor Safety and Related Physics, Chicago, October 5-8, 1976, p. 998.

8. Nuclear Systems Materials Handbook, Property Code 2102, p. 1.0.

9. W. T. Sha and B. E. Launder, A Model for Turbulent Momentum and Heat Transport in Large Rod Bundles, ANL - to be published (1977).

10. A. Whitaker, Advances in Theory of Fluid Motion in Porous Media, Industrial and Engineering Chemistry, Vol. 61, No. 12, (December 1969).

11. M. H. Fontana, R. E. MacPherson, P. A. Gnadt, L. F. Parsly, and J. L. Wantland, Temperature Distribution in a 19-tof Simulated LMFBR Fuel Assembly in a Hexagonal Duct (Fuel Failure Mockup Bundle 2A) - Record of Experimental Data, ORNL-TM-4113 (September 1973).